

Improving Triplet-Triple Annihilation Upconversion Output by a Triplet Mediator Approach: Mechanistic Insights on Homo and Hetero-Annihilation in Three Component Systems

Sunil Kumar Kandappa, Victor Gray*

AUTHOR ADDRESS

Department of Chemistry, Ångström Laboratory, Uppsala University, Box 532, SE-751 20 Uppsala, Sweden

KEYWORDS Triplet-triplet annihilation, photon upconversion, kinetic modelling

ABSTRACT: Triplet-triplet annihilation photon upconversion (TTA-UC) is a promising strategy for converting low-energy photons into higher-energy emission, with potential applications in solar energy harvesting, bioimaging, and photocatalysis. A challenge in TTA-UC systems is minimizing the reabsorption of upconverted photons by the annihilator molecules. To address this, we present a mediator-assisted TTA-UC approach utilizing a neutral mediator molecule to facilitate upconversion in the ultraviolet (UV) region. Our study introduces a protocol employing a benzothiophene-based compound, TIPS-BT, as an energy transfer mediator between the sensitizer 4CzBN and the annihilator TIPS-Naphthalene. Through detailed kinetic modeling, we elucidate the underlying mechanism, highlighting the role of hetero-TTA (triplet-triplet annihilation between the mediator and annihilator). Notably, we report the first estimation of a hetero-TTA rate constant, which exceeds the homo-TTA rate by a factor of two. This work broadens the design space for TTA-UC systems by enabling the use of neutral, non-covalently linked mediators, expanding beyond the conventional reliance on charged or covalently tethered species.

INTRODUCTION

Triplet-triplet annihilation photon upconversion (TTA-UC), a process where the energy of two low energy photons is combined into a photon of high energy, has gained significant attention in recent decades in the context of solar energy harvesting¹⁻⁴ and water splitting.⁵⁻¹¹ TTA-UC offers a way to harvest photons with energy lower than the band gap energy photons, which in a single junction solar cell otherwise would be unutilized. Likewise, high energy photons could be beneficial for photosensitization in water splitting which often relies on materials with high band gap energies. Several other applications¹² include bioimaging,¹³ photodynamic therapy,¹⁴ photoredox catalysis,¹⁵ photocatalytic degradation of volatile organic compounds,¹⁶ in designing soft actuators to induce photomechanical effects,¹⁷ OLEDs^{18,19} and in energy storage devices²⁰.

A typical TTA-UC system consists of a triplet sensitizer molecule which acts as an energy donor and annihilator molecules that act as an energy acceptor. The sensitizer molecule absorbs the incoming low energy photons and eventually populates its triplet state after intersystem crossing (ISC). Triplet formation is followed by triplet energy transfer (TET) to an annihilator molecule. The triplet excited annihilator can combine its triplet energy with that of an adjacent triplet excited annihilator molecule through triplet-triplet annihilation (TTA). TTA populates a higher energy state, which ideally relaxes to the first singlet excited state (S_1), that eventually emits upconverted light. The efficiency of intermolecular TTA process in solutions is curtailed by the diffusion limit of annihilator and sensitizer molecules. Yet, with the long triplet

lifetime and achievable mM concentrations of organic molecules in deaerated organic solvents, TET and TTA can proceed efficiently. Intramolecular TTA-UC is possible when two or more annihilator molecules are linked together and it has gained interest as a means to overcome the diffusion limit.²¹⁻²⁵ However, this approach is associated with the challenge of proper molecular design to achieve efficient TTA, triplet migration and sensitization.²⁶

To ensure an efficient TTA-UC process in solution, a long triplet lifetime of sensitizer and annihilator is essential. The triplet energy transfer efficiency is given by:

$$\eta_{TET} = 1 - \left[\frac{1}{1 + \tau_0 k_Q [Q]} \right] \quad (1)$$

where τ_0 is the triplet lifetime of unquenched sensitizer and k_Q is the bimolecular quenching rate constant with a quencher of concentration $[Q]$. To maximize η_{TET} a typical TTA-UC system usually uses a high concentration of annihilator. However, the high concentration of annihilator molecules subsequently causes an intrinsic challenge where upconverted light will get reabsorbed by the annihilator molecule itself. Reabsorption becomes a major issue especially when the annihilator molecule has a small Stokes shift, which is often the case in the rigid polyaromatic hydrocarbons often used as annihilators. As an example, most reported TTA-UC yields are reported after reabsorption correction and for two traditional UC systems PdOEP/DPA (PdOEP = palladium octaethylporphyrin, DPA = diphenylanthracene) and 4CzBN/TIPS-Nap (4CzBN = 2,3,5,6-tetra(9H-carbazol-9-yl)benzotrile, TIPS-Nap = 1,4-bis[2-[tris(1-

methylethyl)silyl]ethynyl]naphthalene) the difference between reabsorption corrected and non-corrected UC yields can in our experience approach a factor of 2 difference. To avoid reabsorption, lowering the concentration of annihilator molecules as such is also not a viable solution since this would decrease η_{TET} and subsequent TTA. A strategy to maintain a high rate of TET and TTA process with low concentration of annihilator would minimize the reabsorption of upconverted light.

In this regard, recent work has used mediator assisted TTA-UC to bypass some of the obstacles associated with the prototypical TTA-UC involving sensitizers and high concentration of annihilator molecules.^{27–34} Mediator assisted TTA-UC system consists of a third component along with sensitizer and annihilator which acts as a mediator for energy transfer between sensitizer and annihilator (Figure 1). An efficient mediator needs to have a long triplet lifetime and its triplet energy should lie in between that of sensitizer and annihilator. Figure 1 depicts the Jablonski diagram for mediator assisted TTA-UC.

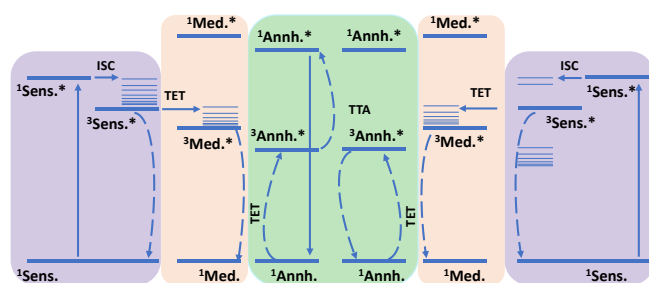


Figure 1: Jablonski diagram for mediator assisted triplet-triplet annihilation upconversion (TTA-UC). Sens., Med., and Ann. refers to sensitizer, mediator and annihilator, respectively.

A few different approaches to using mediators have been reported. Most commonly a mediator is tethered to a sensitizer or quantum dot, effectively extending the apparent triplet lifetime of the sensitizer by ensuring fast TET from sensitizer to mediator.^{27–33} A more recent report from Kerzig and coworkers employed Coulombic interactions³⁴ to increase the rate constant for TET between sensitizer and mediator beyond the diffusion limit without covalent linkage. They emphasized the significance of Coulombic interaction between mediator and annihilator to maintain their proximity. A lower efficiency of TTA-UC was observed for the system without Coulombic interaction compared to that with Coulombic interaction between sensitizer and mediator. They also noted the positive effect of lowering the annihilator concentration for minimizing reabsorption. However, both covalent and Coulombic approaches entail certain limitations. For example, linking a mediator molecule to a sensitizer might involve a tedious synthetic approach. In those cases where sensitizers and mediator molecules are bound by Coulombic interactions, they are limited to only charged species.

A non-covalent mediator approach without Coulombic interactions has been highlighted by Schmidt and co-workers³⁵ in 2016 to minimize the reabsorption from annihilator molecules by reducing its concentration while maintaining high concentration of mediator molecule for an efficient TET transfer process. In their three-component system, they used bis-phenylethynylantracene (BPEA) molecule as mediator for energy transfer from sensitizer PQ4PdNA to annihilator

molecule rubrene. Schmidt and coworkers³⁶ also reported singlet oxygen mediated TTA-UC process with an uncharged annihilator. However, upconversion in the blue region mediated by singlet oxygen is highly unlikely, as it requires annihilator molecules with triplet energies lower than the singlet oxygen energy (0.98 eV). Other three-component TTA-UC systems include those by Balushev and coworkers³⁷ and Zhang and coworkers.³⁸ However, in these cases the same, or similar, concentration was used for two different emitter molecules, hence these are not mediated TTA-UC systems. Furthermore, the impact of reabsorption of upconverted emission is lacking in these reports. Schmidt and Castellano discussed the kinetics of three-component systems in low triplet concentration regimes and emphasized the role of hetero-TTA, i.e. TTA between one mediator and one annihilator, when the triplet concentration of mediator and annihilator are equal.³⁹

In the solid state there are also reports of three-component systems consisting of a sensitizer, annihilator and an emitter molecule which act as a singlet acceptor (often referred to as singlet sink). Singlet energy transfers from annihilator to the emitter molecule has successfully been employed to mitigate singlet fission from annihilator singlets^{40–42} but this approach differs from the triplet mediator approach as highlighted recently by Carrod *et al.*⁴³ In the solids state films studied by Carrod *et al.* tetracene was used as a triplet mediator and rubrene as the annihilator. Monte Carlo simulations explained why, at higher intensities, the ratio between hetero-TTA and homo-TTA of the mediator shifted to favor mediator homo-TTA, which was detrimental for UC output. The reason for majority homo-TTA in the mediator at higher intensities came from the high local concentration of mediator triplets arising from the high intensity excitation and poor triplet migration.

Such limitations have not yet been discussed in solution based three-component systems and to the best of our knowledge, a full mechanistic discussion of the mediator approach in solution has not yet been presented. Furthermore, mediator assisted TTA-UC for UV emitting annihilators is still lacking.

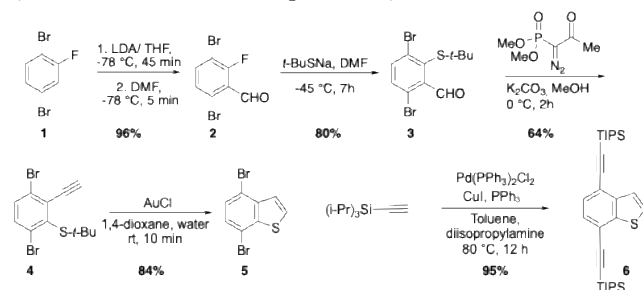
Herein we show a protocol to use a neutral mediator molecule for TTA-UC in the UV region with detailed kinetic modelling, revealing the mechanism involved in the process. In our system benzothiophene based molecule TIPS-BT was used as a mediator with a well-established blue emitting annihilator molecule, TIPS-Nap and sensitizer 4CzBN.^{44,45} TIPS-BT was found to be a perfect choice to act as a mediator molecule with its triplet energy ($T_1 = 2.37$ eV, SI, Figure S22) lying in between that of sensitizer 4CzBN ($T_1 = 2.71$ eV)⁴⁵ and annihilator TIPS-Nap ($T_1 = 2.12$ eV)^{5,45}. Additionally, the singlet energy of TIPS-BT (3.54 eV) is higher than that of TIPS-Nap (3.40 eV, determined from the absorption onset, Figure 2). Hence, the possibility for the former molecule to act as singlet sink is minimized. Instead, it can efficiently act as mediator for triplet energy transfer from sensitizer to annihilator molecule. We were able to achieve over 10-fold increase in the triplet-triplet annihilation upconversion quantum yield (TTA-UC QY) for TIPS-BT mediator assisted upconversion in the presence of 4CzBN sensitizer and TIPS-Nap annihilator compared to the system without mediator while maintaining the same concentration of sensitizer and annihilator (*vide infra*). We were able to reduce the concentration of annihilator almost an order magnitude lower than the typical concentration used for TTA-UC studies using TIPS-Nap annihilator^{44,45} while maintaining

the same order of upconversion QY. Our approach could expand the range of annihilator and mediator molecule for TTA-UC process by not necessarily binding them together by means of covalent linkage or restricting them to be a charged species for Coulombic interactions.

RESULTS AND DISCUSSION

Synthesis

The mediator molecule TIPS-BT was synthesized as per the previous report.^{46,47} 1,4-dibromo-2-fluorobenzene was reacted with LDA in THF at -78 °C for 45 min. This was followed by the addition of dimethylformamide at the same temperature and stirring for 5 minutes resulted in the formation of corresponding aldehyde 3,6-dibromo-2-fluorobenzaldehyde **2** in 96% crude yield.⁴⁷ It was taken as such for the next step without further purification and treated with sodium-2-methyl-2-propanethiolate in DMF at -45 °C for 7 h to form 3,6-dibromo-2-[(1,1-dimethylethyl)thio]benzaldehyde **3** in 80% isolated yield. This was followed by the reaction with dimethyl acetylmethylphosphonate in the presence of K₂CO₃, in methanol at 0 °C for 2 h, resulting in the formation of corresponding alkyne derivative 1,4-dibromo-2-[(1,1-dimethylethyl)thio]-3-ethynyl-benzene **4** in 64% isolated yield. This was further treated with AuCl in dioxane/water mixture (5:1) in rt for 10 min to form 4,7-dibromobenzo[b]thiophene **5** in 84% isolated yield. Sonogashira coupling of this product with (triisopropylsilyl)acetylene resulted in 4,7-bis[2-[tris(1-methylethyl)silyl]ethynyl]-benzo[b]thiophene **6** in 95% isolated yield. We abbreviated this compound as TIPS-BT (refer to SI for the detailed procedure).



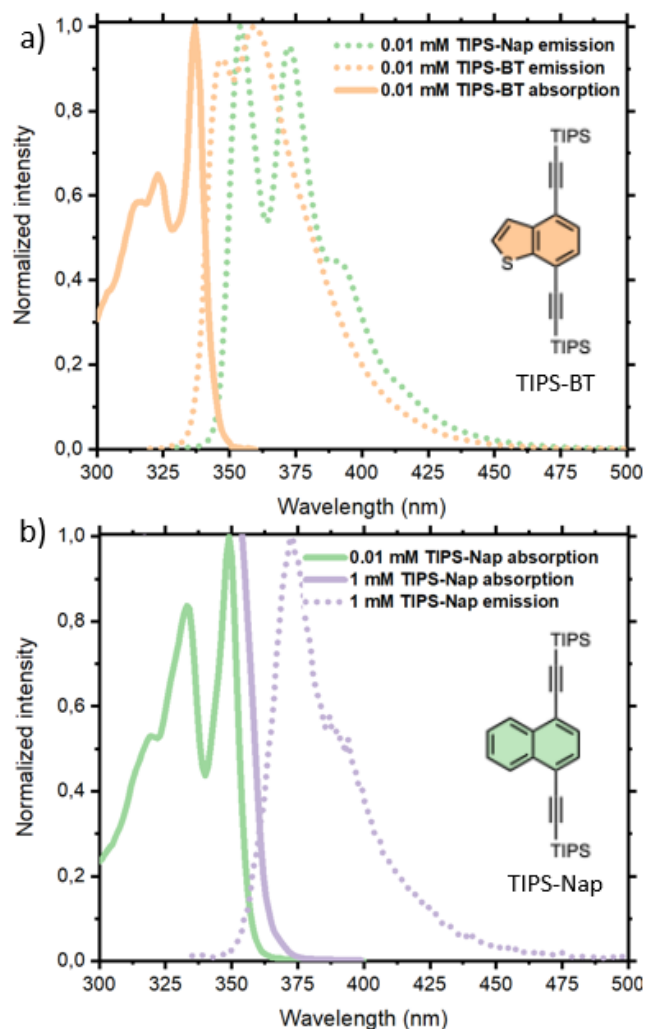
Scheme 1: Synthesis of TIPS-BT

Photophysical characterization

Figure 2a comprises normalized emission spectra of TIPS-Nap, TIPS-BT and UV-Vis absorption spectra of TIPS-BT in toluene. Absorption onset of TIPS-Nap (0.01 mM) is around 365 nm (figure 2b) compared to that of TIPS-BT which is around 350 nm (figure 2a). Importantly, there is minimal spectral overlap between the emission of annihilator TIPS-Nap and absorption of mediator TIPS-BT (346-350 nm). Hence, TIPS-BT can be used as a mediator at high concentration with minimal reabsorption of upconverted emission from TIPS-Nap (*vide infra*). On the other hand, TIPS-Nap exhibits significant reabsorption of emitted light at higher concentration as evident from the decreased intensity of emission peak in the blue region (~354 nm) on increasing its concentration from 0.01 mM (figure 2a, green dotted line) to 1 mM (figure 2b, purple dotted line).

Mediator enhanced upconversion

The mediator assisted TTA-UC process involves two triplet energy transfer (TET) processes. In the first TET from sensitizer to mediator ($TET^{S \rightarrow M}$), mediator TIPS-BT acts as a quencher with respect to the triplet energy of sensitizer 4CzBN. In the second TET process from mediator to annihilator



($TET^{M \rightarrow A}$), the annihilator TIPS-Nap acts as quencher with respect to the triplet energy of mediator. Higher concentration of

Figure 2: **a)** Normalized emission spectra of 0.01 mM TIPS-Nap (dotted green line), 0.01 mM TIPS-BT (dotted orange line) and UV-Vis absorption spectra of 0.01 mM TIPS-BT (solid orange line). **b)** Normalized emission spectra of 1 mM TIPS-Nap (dotted purple line) and normalized UV-Vis absorption spectra of 0.01 mM and scaled UV-Vis absorption spectra 1 mM TIPS-Nap (solid green and purple line).

mediator increases the efficiency of $TET^{S \rightarrow M}$ (Eq. 1), and since TIPS-BT absorption exhibits minor overlap with the emission spectra of annihilator TIPS-Nap it is possible to use TIPS-BT in high concentration with minimal reabsorption of upconverted light by the mediator. On the other hand, higher η_{TET} for $TET^{M \rightarrow A}$ is accomplished by choosing a mediator with relatively high triplet lifetime. The concentration of TIPS-Nap was maintained at minimal level to reduce the intrinsic reabsorption by the annihilator molecule.

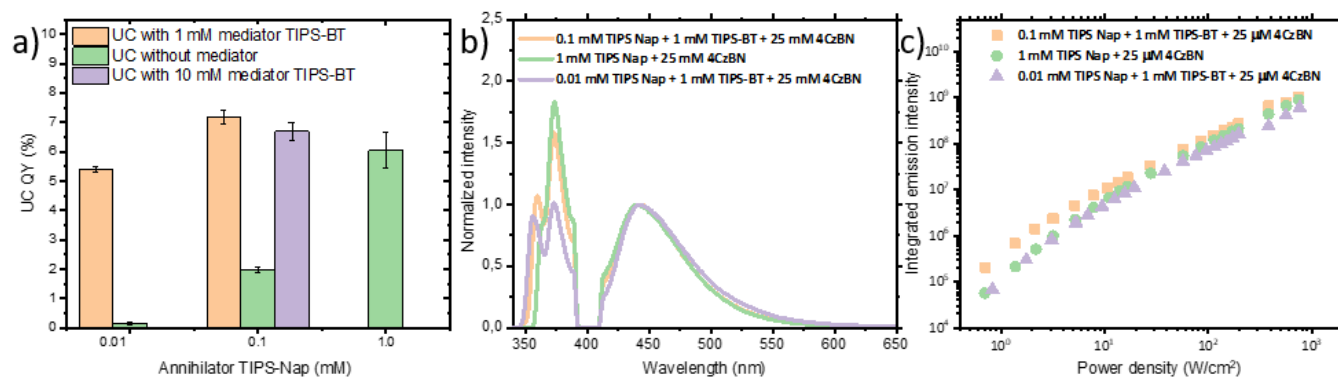


Figure 3: a) Comparison of TTA-UC quantum yield for systems with sensitizer 4CzBN (25 μM) and annihilator TIPS-Nap at three different concentrations (0.01 mM, 0.1 mM and 1 mM) in the presence and absence of mediator. Error bar for 1 mM TIPS-Nap and 0.1 mM TIPS-Nap in the presence of 1 mM TIPS-BT is the standard deviation measured over four independent measurements. For the rest of the sample error bars indicates spread over two independent measurements. b) TTA-UC emission spectra for bi- and tri-component systems, excited at 405 nm with a power density of 830 W/cm^2 . Spectra are normalized to the sensitizer emission intensity. c) Plot of the upconverted emission intensity as a function of excitation power density.

For the detailed analysis of TIPS-BT mediator assisted TTA-UC studies, we vary the TIPS-Nap annihilator concentration from 0.1 mM to 0.01 mM while maintaining the concentration of sensitizer at 25 μM and mediator at 1 mM. The TTA-UC QY from the three-component system is compared to the corresponding two component system (annihilator and sensitizer only). All solutions are prepared in vacuum degassed toluene (5-cycles). Lowering the concentration of TIPS-Nap from 1 mM to 0.1 mM in the upconversion mixture results in the UV-Vis absorption onset around 373 nm to blue shift by about 10 nm (Figure S14, SI). Similarly, fluorescence of TIPS-Nap blue shifts (Figure S21, SI) due to minimized reabsorption in the upconversion mixture with 0.1 mM TIPS-Nap compared to that of the case with 1 mM TIPS-Nap. Figure 3 summarizes comparison of TTA-UC QYs without reabsorption correction (practical output flux of upconverted light). TTA-UC QYs before reabsorption correction are considered for the discussion below. For comparison, TTA-UC QYs after reabsorption correction are included in Table S1, SI. TTA-UC with 25 μM 4CzBN, 1 mM TIPS-BT and 0.1 mM TIPS-Nap mixture shows a TTA-UC QY of $7.2 \pm 0.3\%$ (Figure 3 and SI, Table S1, entry 3) which is almost 4 times higher compared to the system without mediator (*i.e.* 25 μM 4CzBN and 0.1 mM TIPS-Nap). In the absence of mediator TTA-UC QY was $2.0 \pm 0.1\%$ (Figure 3 and SI, Table S1, entry 4). It is noteworthy to mention that TTA-UC QY with 25 μM 4CzBN, 1 mM TIPS-BT and 0.1 mM TIPS-Nap is slightly higher ($7.2 \pm 0.3\%$) than that of the traditional two-component system with higher concentration of annihilator *i.e.* 1 mM TIPS-Nap and 25 μM 4CzBN, ($6.05 \pm 0.5\%$), (Figure 3 and SI, Table S1, entry 1 and entry 3). Lowering the concentration of annihilator further, to only 0.01 mM TIPS-Nap, with 1 mM TIPS-BT mediator, the TTA-UC QY decreases slightly to $5.4 \pm 0.1\%$ (Figure 3 and SI, Table S1, entry 5). Yet, in the absence of mediator the TTA-UC QY with 0.01 mM TIPS-Nap was a mere $0.15 \pm 0.02\%$ (Figure 3 and SI, Table S1, entry 6).

The importance of reabsorption can be illustrated by comparing the measured TTA-UC QY with the reabsorption corrected values. For the two-component system with 1 mM TIPS-Nap reabsorption accounts for a 52% loss in intensity as the corrected TTA-UC QY is $12.6 \pm 0.3\%$ compared to $6.05 \pm 0.5\%$ before correction (SI, Table S1, entry 1). For the three-component system with 0.1 mM TIPS-Nap reabsorption

accounts for 41% signal loss (SI, Table S1, entry 3) and with 0.01 mM TIPS-Nap the reabsorption loss is only 31% (SI, Table S1, entry 5). The fact that there is still 31% reabsorption in the low concentration sample can be explained by the absorption overlap of the sensitizer in the emission region (SI, Figure 21).

On increasing the concentration of mediator TIPS-BT to 10 mM, while maintaining the concentration of sensitizer at 25 μM and annihilator at 0.1 mM, no significant change in the upconversion QY is observed *i.e.* $6.7 \pm 0.3\%$ (Figure 3 and SI, Table S1, entry 9).

To investigate whether the mediator itself is undergoing TTA-UC and contributing to the overall upconversion efficiency TTA-UC experiments with 1 mM TIPS-BT and 25 μM 4CzBN were performed. The TTA-UC QY for the 1 mM TIPS-BT and 25 μM 4CzBN systems is approximately 6.5 times lower ($1.0 \pm 0.1\%$) than 1 mM TIPS-Nap and 25 μM 4CzBN. This low TTA-UC QY is attributed to the ~ 6 times lower fluorescence QY of TIPS-BT (11.9% in toluene), compared to that of TIPS-Nap (77% in toluene⁴⁵). The low emission QY from the mediator, yet high TTA-UC QY from the three-component system suggests that homo-TTA of the mediator is a minor problem and that TIPS-BT indeed acts as a mediator for energy transfer from sensitizer to annihilator.

To understand the generality of the mediator approach, we switch the mediator to 1,4-bis[2-[tris(1-methylethyl)silyl]ethynyl]benzene, TIPS-Ph. The triplet energy of TIPS-Ph is 2.64 eV⁴⁸ slightly higher than TIPS-BT ($T_1 = 2.37$ eV) but still in between that of 4CzBN ($T_1 = 2.71$ eV) and TIPS-Nap ($T_1 = 2.12$ eV) complying the requirement for mediator for triplet energy transfer. The concentration of annihilator and sensitizer is maintained at the same level as that of the best TTA-UC system with 1 mM mediator TIPS-BT *i.e.* 0.1 mM TIPS-Nap and 25 μM 4CzBN. The concentration of TIPS-Ph was maintained at 1 mM. Under this condition TTA-UC QY is quite low, $3.0 \pm 0.2\%$ (Figure 3 and SI, Table S1, entry 10). Yanai and co-workers⁴⁸ reported TIPS-Ph as an annihilator for TTA-UC in the presence of 4CzBN sensitizer with TTA-UC QY of 1%, albeit at high concentration 10 mM of annihilator, suggesting that TET from 4CzBN to TIPS-Ph might not be as efficient as for the TIPS-Nap. Nevertheless, given that the TTA-UC system with TIPS-Ph mediator shows a higher TTA-UC QY (Figure 3 and SI, Table S1, entry 10) compared to the TTA-UC QY of the

two-component system with only 0.1 mM TIPS-Nap (Figure 3 and

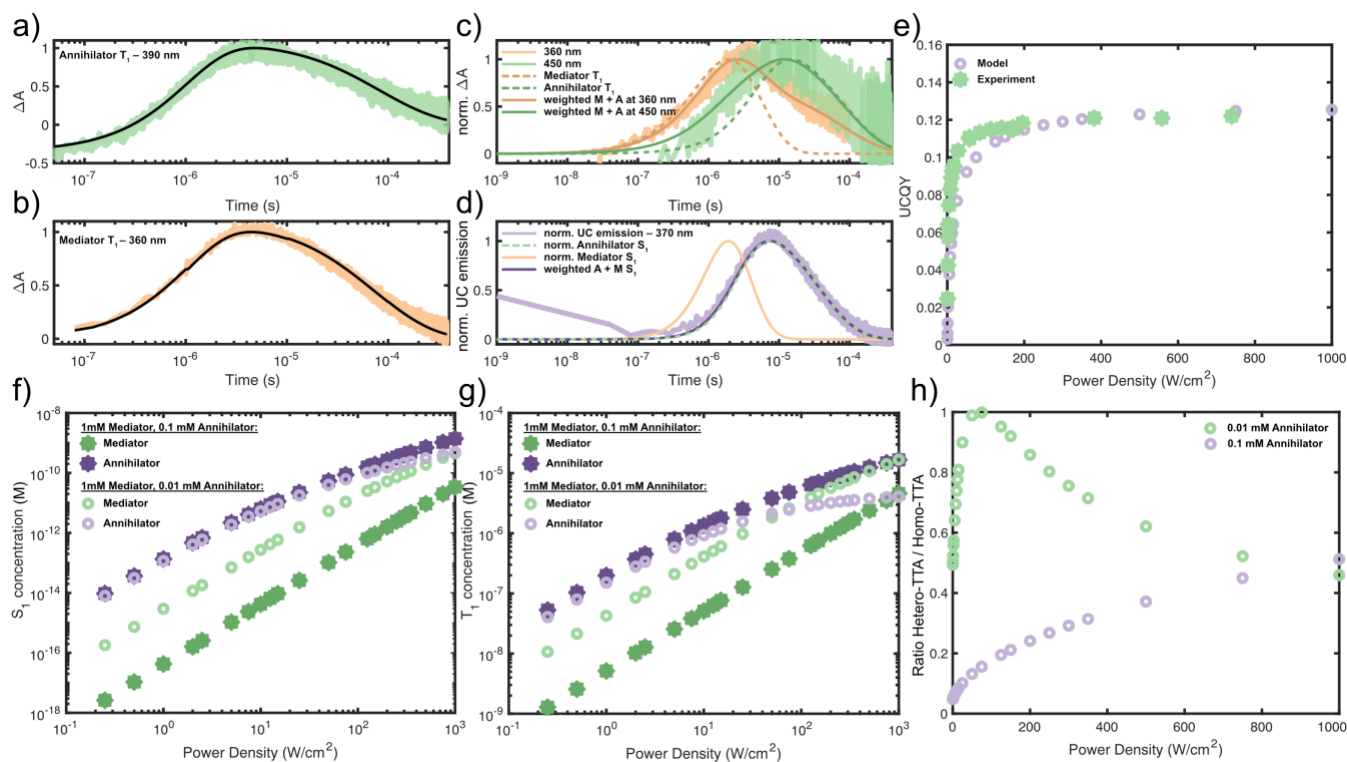


Figure 4. Time profile of the triplet excited state absorption for a) TIPS-Nap at 390 nm and b) TIPS-BT at 360 nm in samples with 25 μM 4CzBN and either 1 mM TIPS-Nap or TIPS-BT, excited at 410 nm with 2.3 mJ/pulse. c) Time profiles at 360 nm (orange) and 450 nm (green) of a sample containing 25 μM 4CzBN, 1 mM TIPS-BT and 0.1 mM TIPS-Nap, with the same excitation conditions as in a) and b). Trace at 360 nm corresponds to majority TIPS-BT triplet absorption and traces at 450 nm mostly TIPS-Nap triplet absorption. Dashed lines are modelled triplet populations and solid lines are weighted sums of both TIPS-Nap and TIPS-BT triplet populations. d) Kinetic trace of upconverted emission detected at 370 nm for the same conditions as in c). Solid lines indicate normalized population dynamics of mediator and annihilator singlet states (S_1), and the dashed line a fluorescence QY weighted sum of the mediator and annihilator S_1 populations. e) Experimental (solid green) and modelled (open purple) upconversion quantum yields as a function of excitation power density for 25 μM 4CzBN, 1 mM TIPS-BT and 0.1 mM TIPS-Nap. f) modelled S_1 population as a function of excitation power density for high (0.1 mM, solid) and low (0.01 mM, open) concentrations of TIPS-Nap annihilator with 1 mM TIPS-BT mediator and 25 μM 4CzBN. g) as in f) but triplet excited state (T_1) population of mediator (green) and annihilator (purple) species. h) The ratio of hetero-TTA and the sum of annihilator and mediator homo-TTA as a function of excitation power density for low (0.01 mM, green) and high (0.1 mM, purple) concentrations of annihilator.

SI, Table S1, entry 4), indicates that TIPS-Ph does act as a mediator, but with less efficiency compared to that of TIPS-BT. Contribution of TTA-UC from TIPS-Ph itself is also minimized in the mixture of 25 μM 4CzBN, 1 mM TIPS-Ph and 0.1 mM TIPS-Nap as TIPS-Ph needs to be in higher concentration (10 mM) to undergo efficient TTA-UC as per the previous report from Yanai and co-workers.⁴⁸ It is evident from Table S1, TIPS-BT acts as better mediator compared to TIPS-Ph (Figure 3 and SI, Table S1, entry 10) under the same concentration of sensitizer and annihilator. Since the absorbance of TIPS-Ph and TIPS-BT looks nearly identical (Figure S15, SI) it is unlikely that the lower efficiency of TIPS-Ph as a triplet mediator arises due to greater reabsorption of upconverted emission by TIPS-Ph. Instead, it is likely due to slower and less efficient $TET^{S \rightarrow M}$ as reported previously ($k_{TET} \sim 6 \times 10^7 \text{ M}^{-1} \text{ s}^{-2}$).⁴⁸

Mechanistic insights to mediator enhanced TTA

We use nanosecond-to-millisecond flash photolysis to gain further insights into the mediator enhanced TTA-UC process. First, the mediator and annihilator are studied along with

4CzBN as sensitizer. Figure 4a and b show the kinetics associated with the TIPS-Nap (annihilator) and TIPS-BT (mediator) triplets. Fitting the kinetic profile according to conventional TTA-UC kinetics (Ref.^{49,50}, see details in SI Section 10) with the TTA rate constant (k_{TTA}) as the sole fitting parameter indicates that both TIPS-Nap and TIPS-BT have similar k_{TTA} of about $1 \times 10^9 \text{ M}^{-1} \text{ s}^{-1}$. With k_{TTA} and the experimental threshold intensity (I_{th}) we then extract the triplet lifetimes according to equation 2:

$$I_{th} = \frac{k_T^2}{2k_{TTA}\alpha[\text{Sens}]} \quad (2)$$

Where k_T is the inverse of the triplet lifetime, α is the absorption cross-section of the sensitizer at the excitation wavelength, and $[\text{Sens}]$ is the sensitizer concentration.

We observe that the triplet lifetime of TIPS-BT (156 μs) is slightly shorter than TIPS-Nap (194 μs), perhaps due to the incorporation of the slightly heavier sulphur atom in the structure.

Importantly, the model works well to reproduce both the kinetic traces, the reabsorption corrected steady-state TTA-UC QYs and intensity ramps for the bimolecular systems (Figures S35 and S36). We then extend the model to a three-component system where we consider: triplet energy transfer from the sensitizer to both mediator and annihilator; triplet energy transfer from mediator to annihilator; homo-TTA between either two triplet excited mediators or two triplet excited annihilators; as well as hetero-TTA between one triplet excited mediator and one triplet excited annihilator. The full kinetic model is described in the SI.

Flash photolysis measurements of the three-component system (25 μM 4CzBN, 1 mM TIPS-BT, 0.1 mM TIPS-Nap) show an initial rise of the mediator triplet followed by a delayed population of the annihilator triplet state, Figure 4c. These trends can be reproduced with the kinetic model using rate constants (k_{TTA} and k_{TET}) for the mediator and annihilator determined from the individual measurements.

We also look at the delayed UC emission and find that the UC emission peaks at 10 μs Figure 4d. Since UC emission will result from the population of either the mediator or annihilator singlet excited state (S_1) we compare the UC time profile to our model. The kinetic model predicts early population of mediator S_1 , maximizing at 1 μs . Furthermore, in the steady-state UC measurements we only observe annihilator fluorescence, leading us to conclude that the UC signal arises from annihilator emission. Without hetero-TTA in the model the annihilator S_1 reaches a maximum at a longer time scale than what is observed (16 μs). Introducing a hetero-TTA channel with $k_{\text{TTA-hetero}} = 2k_{\text{TTA-homo}}$ yields an excellent match with the time profile, Figure 3d. At this stage it is unclear why hetero-TTA would have a larger rate constant than homo-TTA, perhaps it is due to the slightly larger driving force for TTA when a higher energy mediator triplet is consumed to populate the annihilator singlet. Cao et al.³⁸ saw a lowering of the excitation intensity dependence on the UC emission in three-component systems, yet no satisfactory explanation has been presented. However, their observations are in line with an increased rate constant of hetero-TTA compared to homo-TTA, as suggested by our model.

As an alternative to hetero-TTA, singlet annihilators could be populated from singlet energy transfer (SET) from mediator singlets. However, to fit the experimental UC time-profile a SET rate constant $>10^{13} \text{ M}^{-1}\text{s}^{-1}$ is required which is far beyond the diffusion limit. Furthermore, the shape of the annihilator S_1 kinetics becomes broader than what is observed experimentally. Additionally, considering the low fluorescence QY of the mediator TIPS-BT, the TTA-UC QYs would be reduced if the main annihilator S_1 population pathway was through SET. We thus only include the hetero-TTA channel in our further analysis. For example, the model also yields excellent agreement to the experimental steady-state TTA-UC QY measurements, Figure 4e and S37.

With a satisfactory model, we now use it to shed further mechanistic insight to mediator enhanced TTA and compare to previous reports in the literature. In 2023 Glaser et al.³⁴ demonstrated a mediator enhanced TTA-UC system using Coulomb interactions to increase the sensitizer to mediator triplet energy transfer rate constant ($k_{\text{TET}}^{\text{S}\rightarrow\text{M}}$) beyond the diffusion limit. In Figure 5 we show the effect of varying $k_{\text{TET}}^{\text{S}\rightarrow\text{M}}$ for different systems. In our system with 1 mM mediator and 0.1 mM annihilator there is little benefit of

increasing the triplet energy transfer rate from $10^9 \text{ M}^{-1}\text{s}^{-1}$ to $10^{10} \text{ M}^{-1}\text{s}^{-1}$. Yet, in a situation where the sensitizer lifetime is 10 times shorter (600 ns), there is a 3 times enhancement in UCQY with the same change. Furthermore, with a larger $k_{\text{TET}}^{\text{S}\rightarrow\text{M}}$ a lower mediator concentration can be used to achieve the same UC efficiency. Similar analysis, but varying the rate constants for intrinsic triplet decay of the mediator (k_{T}^{BT}) or sensitizer (k_{T}^{S}), the rate constants for hetero or homo-TTA ($k_{\text{TTA-hetero}}$ and $k_{\text{TTA-homo}}$, respectively), (Figure

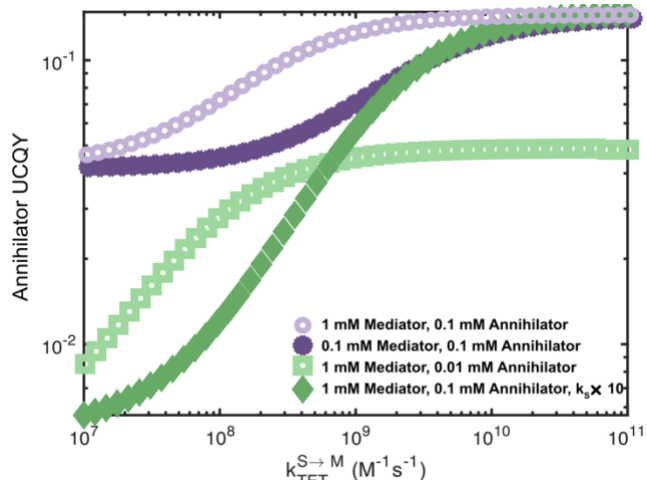


Figure 5. Modelled upconversion quantum yield originating from annihilator emission as a function of sensitizer to mediator triplet energy transfer (TET) rate constant ($k_{\text{TET}}^{\text{S}\rightarrow\text{M}}$) for 4 different trimolecular systems. $k_{\text{S}}\times 10$ refers to the case with a 10 times shorter sensitizer triplet lifetime, here 600 ns.

S39) indicate that the current system is close to optimal, and shorter triplet lifetimes and slower TTA will have a negative effect on the UC efficiency, as can be deduced for the corresponding bimolecular TTA-UC systems.

Another interesting comparison is to that of a mediator enhanced TTA-UC system in the solid state using rubrene as annihilator and tetracene as mediator, reported by Carrod et al.⁴³ They found that hetero-TTA decreased with excitation intensity as the local mediator triplet concentration ($[^3\text{M}^*]$) increased and led to increased mediator homo-TTA. In solution with efficient triplet migration through diffusion homo-TTA of the mediator is expected to be less of an issue.

In solution, we find that hetero-TTA is more important at low annihilator concentrations (0.01 mM annihilator, Figure 4h). Hetero-TTA and TTA-UC QY are maximized when annihilator and mediator triplet concentrations are equal, as predicted by Schmidt and Castellano³⁹ (Figure 4g and h, and S38). However, in their analysis their analytical solutions were limited to low excitation intensity regions where triplet decay mainly occurs through intrinsic decay. With 0.1 mM annihilator TET is sufficiently efficient to keep $[^3\text{A}^*]$ well above $[^3\text{M}^*]$ and consequently annihilator homo-TTA dominates at intensities below $10\,000 \text{ W/cm}^2$ (Figure S40).

Similarly, at low intensities TTA is inefficient due to low $[^3\text{M}^*]$ and $[^3\text{A}^*]$, resulting in TET from mediator to annihilator to dominate the $[^3\text{M}^*]$ decay for both 0.1 mM and 0.01 mM annihilator concentrations. Consequently, homo-TTA of $[^3\text{A}^*]$ is the main source of UC emission, Figure 4f. At low annihilator concentration (0.01 mM) but higher intensities the $[^3\text{A}^*]$

concentration saturates as the annihilator ground state population is depleted significantly and mediator to annihilator TET levels off. Instead [$^3M^*$] increases and mediator homo-TTA and hetero-TTA dominates over annihilator homo-TTA. Due to the low fluorescence quantum yield of the mediator, homo-TTA of $^1M^*$ will result in ~6 times lower TTA-UC QY compared to the same [$^1A^*$]. Hence when [$^1M^*$] dominates in Figure 4f it translates to a decrease in the TTA-UC QY due to mediator homo-TTA, as observed experimentally Figure S37.

On the other hand, at high (0.1 mM) annihilator concentrations [$^1A^*$] dominates over [$^1M^*$] due to efficient annihilator homo-TTA, Figure 4f. For low annihilator concentrations (0.01 mM) [$^1A^*$] is the majority product until about 750 W/cm², when [$^1M^*$] crosses over and becomes the dominant product. This crossover occurs at much higher excitation densities than where [$^3M^*$] becomes dominant (Figure 4g), thanks to efficient hetero-TTA still yielding [$^1A^*$]. At intensities beyond 1000 W/cm² (0.01 mM annihilator) mediator homo-TTA is expected to dominate fully, analogous to the solid-state case reported by Carrod et al.⁴³ With a higher annihilator concentration (0.1 mM) the leveling off of [$^3A^*$] due to annihilator ground state depletion is slower and requires a significantly higher intensity, beyond what our experimental setup can achieve. Yet with a stronger sensitizer absorption, one might approach such regimes also in solution.

CONCLUSIONS

Herein we demonstrate a three-component upconversion system comprising a sensitizer, an annihilator and a triplet mediator. The triplet mediator ensures efficient triplet energy transfer from sensitizer to annihilator, allowing us to reduce the annihilator concentration by a factor of 100 which in turn reduces the intrinsic reabsorption of the system from 50% to 31%. Our approach increases the range of possible sensitizer and mediator molecules by not restricting them to charged species with Coulombic interactions or covalently linked dyads. We also present a detailed mechanistic model and evaluate the rate-constant for hetero-TTA (TTA between a mediator and an annihilator). To the best of our knowledge this is the first time a hetero-TTA rate constant has been estimated. Importantly, the rate constant of hetero-TTA appears to be larger than the homo-TTA rate constants, possibly due to a larger energetic driving force for TTA. Overall, this work presents a mechanistic basis to further explore mediator enhanced TTA-UC systems.

ASSOCIATED CONTENT

Supporting Information

Supporting Information is available online with additional experimental details, data and details for the synthesis, additional fluorescence and absorption spectra, details on the kinetic modelling. Data underlying the figures and conclusions in this publication, including the MATLAB code is available at Zenodo data repository at: [link to be added during proof](#)

AUTHOR INFORMATION

Corresponding Author

* Victor Gray, e-mail: victor.gray@kemi.uu.se.

Author Contributions

Both authors contributed to the writing and have given approval to the final version of the manuscript.

Funding Sources

Swedish research council (VR – grant 2021-03744)
Carl Trygger Foundation for Scientific Research (CTS 22:1911).

ACKNOWLEDGMENT

The authors acknowledge funding from the Swedish research council (VR – grant 2021-03744) and the Carl Trygger Foundation for Scientific Research (CTS 22:1911). HRMS experiments were performed at Science for Life Laboratory, Spatial Mass Spectrometry, Uppsala University, Uppsala, Sweden.

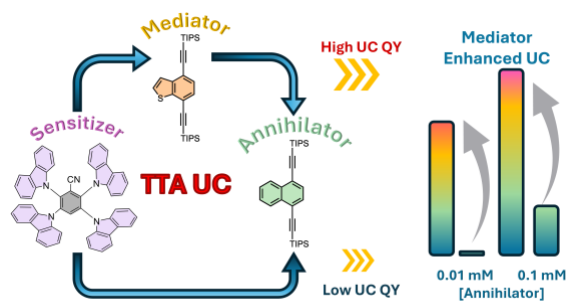
REFERENCES

- (1) Gray, V.; Moth-Poulsen, K.; Albinsson, B.; Abrahamsson, M. Towards Efficient Solid-State Triplet–Triplet Annihilation Based Photon Upconversion: Supramolecular, Macromolecular and Self-Assembled Systems. *Coordination Chemistry Reviews* **2018**, *362*, 54–71. <https://doi.org/10.1016/j.ccr.2018.02.011>.
- (2) Trupke, T.; Shalav, A.; Richards, B. S.; Würfel, P.; Green, M. A. Efficiency Enhancement of Solar Cells by Luminescent Up-Conversion of Sunlight. *Solar Energy Materials and Solar Cells* **2006**, *90* (18), 3327–3338. <https://doi.org/10.1016/j.solmat.2005.09.021>.
- (3) Ekins-Daukes, N. J.; Schmidt, T. W. A Molecular Approach to the Intermediate Band Solar Cell: The Symmetric Case. *Applied Physics Letters* **2008**, *93* (6), 063507. <https://doi.org/10.1063/1.2970157>.
- (4) Schulze, T. F.; Schmidt, T. W. Photochemical Upconversion: Present Status and Prospects for Its Application to Solar Energy Conversion. *Energy Environ. Sci.* **2015**, *8* (1), 103–125. <https://doi.org/10.1039/C4EE02481H>.
- (5) Harada, N.; Sasaki, Y.; Hosoyamada, M.; Kimizuka, N.; Yanai, N. Discovery of Key TIPS-Naphthalene for Efficient Visible-to-UV Photon Upconversion under Sunlight and Room Light. *Angewandte Chemie International Edition* **2021**, *60* (1), 142–147. <https://doi.org/10.1002/anie.202012419>.
- (6) Chandrasekaran, S.; Ngo, Y.-L. T.; Sui, L.; Kim, E. J.; Dang, D. K.; Chung, J. S.; Hur, S. H. Highly Enhanced Visible Light Water Splitting of CdS by Green to Blue Upconversion. *Dalton Trans.* **2017**, *46* (40), 13912–13919. <https://doi.org/10.1039/C7DT02936E>.
- (7) Yu, T.; Liu, Y.; Zeng, Y.; Chen, J.; Yang, G.; Li, Y. Triplet–Triplet Annihilation Upconversion for Photocatalytic Hydrogen Evolution. *Chemistry – A European Journal* **2019**, *25* (71), 16270–16276. <https://doi.org/10.1002/chem.201904025>.
- (8) Madbak, E.; Osborn, D. J.; Small, T.; Ishwara, T.; Schmidt, T. W.; Domen, K.; Metha, G. F. Utilising Triplet–Triplet Annihilation Upconversion for Overall Photocatalytic Water Splitting. *Chem. Commun.* **2025**, *61* (1), 157–160. <https://doi.org/10.1039/D4CC03961K>.
- (9) Magazov, Y.; Kudryashov, V.; Moldabekov, K.; Amze, M.; Nurmanova, A.; Aliyev, A.; Nuraje, N. Copper Oxide Coupled with Photon Upconversion for Solar Water Splitting. *Communications Materials* **2024**, *5* (1), 126. <https://doi.org/10.1038/s43246-024-00574-5>.
- (10) Liu, S.; Liu, H.; Hu, Y.; Zhao, C.; Huang, H.; Yu, G.; Li, Z.; Liu, Z.; Chen, Y.; Li, X. Boosting Photocatalytic Hydrogen Evolution via Triplet–Triplet Annihilation Upconversion. *Chemical Engineering Journal* **2023**, *452*, 139203. <https://doi.org/10.1016/j.cej.2022.139203>.
- (11) Méndez-Ramos, J.; Borges, M. E.; Torres-García, S.; Medina-Alayón, M.; Acosta-Mora, P.; del-Castillo, J.; Menéndez-Velázquez, A.; García-Delgado, A. B.; Mullins, C. B.; Esparza, P. “There Is Plenty of Energy at the Bottom”: A Spectral Conversion Approach for Upconversion-Powered Water-Splitting PEC Cell. *Journal of Power Sources* **2025**, *625*, 235668. <https://doi.org/10.1016/j.jpowsour.2024.235668>.
- (12) Seo, S. E.; Choe, H.-S.; Cho, H.; Kim, H.; Kim, J.-H.; Kwon, O. S. Recent Advances in Materials for and Applications of Triplet–Triplet Annihilation-Based Upconversion. *J. Mater. Chem. C* **2022**, *10* (12), 4483–4496. <https://doi.org/10.1039/D1TC03551G>.

- (13) Mattiello, S.; Monguzzi, A.; Pedrini, J.; Sassi, M.; Villa, C.; Torrente, Y.; Marotta, R.; Meinardi, F.; Beverina, L. Self-Assembled Dual Dye-Doped Nanosized Micelles for High-Contrast Up-Conversion Bioimaging. *Advanced Functional Materials* **2016**, *26* (46), 8447–8454. <https://doi.org/10.1002/adfm.201603303>.
- (14) Zhang, P.; Steelant, W.; Kumar, M.; Scholfield, M. Versatile Photosensitizers for Photodynamic Therapy at Infrared Excitation. *J. Am. Chem. Soc.* **2007**, *129* (15), 4526–4527. <https://doi.org/10.1021/ja0700707>.
- (15) Ravetz, B. D.; Pun, A. B.; Churchill, E. M.; Congreve, D. N.; Rovis, T.; Campos, L. M. Photoredox Catalysis Using Infrared Light via Triplet Fusion Upconversion. *Nature* **2019**, *565* (7739), 343–346. <https://doi.org/10.1038/s41586-018-0835-2>.
- (16) Kim, H.; Weon, S.; Kang, H.; Hagstrom, A. L.; Kwon, O. S.; Lee, Y.-S.; Choi, W.; Kim, J.-H. Plasmon-Enhanced Sub-Bandgap Photocatalysis via Triplet–Triplet Annihilation Upconversion for Volatile Organic Compound Degradation. *Environ. Sci. Technol.* **2016**, *50* (20), 11184–11192. <https://doi.org/10.1021/acs.est.6b02729>.
- (17) Jiang, Z.; Xu, M.; Li, F.; Yu, Y. Red-Light-Controllable Liquid-Crystal Soft Actuators via Low-Power Excited Upconversion Based on Triplet–Triplet Annihilation. *J. Am. Chem. Soc.* **2013**, *135* (44), 16446–16453. <https://doi.org/10.1021/ja406020r>.
- (18) Di, D.; Yang, L.; Richter, J. M.; Meraldi, L.; Altamimi, R. M.; Alyamani, A. Y.; Credgington, D.; Musselman, K. P.; MacManus-Driscoll, J. L.; Friend, R. H. Efficient Triplet Exciton Fusion in Molecularly Doped Polymer Light-Emitting Diodes. *Advanced Materials* **2017**, *29* (13), 1605987. <https://doi.org/10.1002/adma.201605987>.
- (19) Kukhta, N. A.; Matulaitis, T.; Volyniuk, D.; Ivaniuk, K.; Turyk, P.; Stakhira, P.; Grazulevicius, J. V.; Monkman, A. P. Deep-Blue High-Efficiency TTA OLED Using Para- and Meta-Conjugated Cyanotriphenylbenzene and Carbazole Derivatives as Emitter and Host. *J. Phys. Chem. Lett.* **2017**, *8* (24), 6199–6205. <https://doi.org/10.1021/acs.jpcclett.7b02867>.
- (20) Börjesson, K.; Dzebo, D.; Albinsson, B.; Moth-Poulsen, K. Photon Upconversion Facilitated Molecular Solar Energy Storage. *J. Mater. Chem. A* **2013**, *1* (30), 8521–8524. <https://doi.org/10.1039/C3TA12002C>.
- (21) Yu, S.; Zeng, Y.; Chen, J.; Yu, T.; Zhang, X.; Yang, G.; Li, Y. Intramolecular Triplet–Triplet Energy Transfer Enhanced Triplet–Triplet Annihilation Upconversion with a Short-Lived Triplet State Platinum(II) Terpyridyl Acetylphos Photosensitizer. *RSC Adv.* **2015**, *5* (86), 70640–70648. <https://doi.org/10.1039/C5RA12579K>.
- (22) Dzebo, D.; Börjesson, K.; Gray, V.; Moth-Poulsen, K.; Albinsson, B. Intramolecular Triplet–Triplet Annihilation Upconversion in 9,10-Diphenylanthracene Oligomers and Dendrimers. *J. Phys. Chem. C* **2016**, *120* (41), 23397–23406. <https://doi.org/10.1021/acs.jpcc.6b07920>.
- (23) Edhborg, F.; Küçüköz, B.; Gray, V.; Albinsson, B. Singlet Energy Transfer in Anthracene–Porphyrin Complexes: Mechanism, Geometry, and Implications for Intramolecular Photon Upconversion. *J. Phys. Chem. B* **2019**, *123* (46), 9934–9943. <https://doi.org/10.1021/acs.jpcc.9b07991>.
- (24) Edhborg, F.; Bildirir, H.; Bharmoria, P.; Moth-Poulsen, K.; Albinsson, B. Intramolecular Triplet–Triplet Annihilation Photon Upconversion in Diffusionally Restricted Anthracene Polymer. *J. Phys. Chem. B* **2021**, *125* (23), 6255–6263. <https://doi.org/10.1021/acs.jpcc.1c02856>.
- (25) Mattiello, S.; Mecca, S.; Ronchi, A.; Calascibetta, A.; Mattioli, G.; Pallini, F.; Meinardi, F.; Beverina, L.; Monguzzi, A. Diffusion-Free Intramolecular Triplet–Triplet Annihilation in Engineered Conjugated Chromophores for Sensitized Photon Upconversion. *ACS Energy Lett.* **2022**, *7* (8), 2435–2442. <https://doi.org/10.1021/acsenerylett.2c01224>.
- (26) Olesund, A.; Gray, V.; Mårtensson, J.; Albinsson, B. Diphenylanthracene Dimers for Triplet–Triplet Annihilation Photon Upconversion: Mechanistic Insights for Intramolecular Pathways and the Importance of Molecular Geometry. *J. Am. Chem. Soc.* **2021**, *143* (15), 5745–5754. <https://doi.org/10.1021/jacs.1c00331>.
- (27) Lu, Y.; Wang, J.; McGoldrick, N.; Cui, X.; Zhao, J.; Caverly, C.; Twamley, B.; Ó Máille, G. M.; Irwin, B.; Conway-Kenny, R.; Draper, S. M. Iridium(III) Complexes Bearing Pyrene-Functionalized 1,10-Phenanthroline Ligands as Highly Efficient Sensitizers for Triplet–Triplet Annihilation Upconversion. *Angewandte Chemie International Edition* **2016**, *55* (47), 14688–14692. <https://doi.org/10.1002/anie.201608442>.
- (28) Liu, S.; Wang, X.; Liu, H.; Shen, L.; Zhao, D.; Li, X. Enhancing Triplet Sensitization Ability of Donor–Acceptor Dyads via Intramolecular Triplet Energy Transfer. *J. Mater. Chem. C* **2020**, *8* (10), 3536–3544. <https://doi.org/10.1039/C9TC06337D>.
- (29) Chen, Q.; Liu, Y.; Guo, X.; Peng, J.; Garakyaraghi, S.; Papa, C. M.; Castellano, F. N.; Zhao, D.; Ma, Y. Energy Transfer Dynamics in Triplet–Triplet Annihilation Upconversion Using a Bichromophoric Heavy-Atom-Free Sensitizer. *J. Phys. Chem. A* **2018**, *122* (33), 6673–6682. <https://doi.org/10.1021/acs.jpca.8b05901>.
- (30) Li, H.; Wang, C.; Glaser, F.; Sinha, N.; Wenger, O. S. Metal–Organic Bichromophore Lowers the Upconversion Excitation Power Threshold and Promotes UV Photoreactions. *J. Am. Chem. Soc.* **2023**, *145* (20), 11402–11414. <https://doi.org/10.1021/jacs.3c02609>.
- (31) Niihori, Y.; Kosaka, T.; Negishi, Y. Triplet–Triplet Annihilation-Based Photon Upconversion Using Nanoparticles and Nanoclusters. *Mater. Horiz.* **2024**, *11* (10), 2304–2322. <https://doi.org/10.1039/D4MH00117F>.
- (32) Gray, V.; Toolan, D. T. W.; Dowland, S.; Allardice, J. R.; Weir, M. P.; Zhang, Z.; Xiao, J.; Klimash, A.; Winkel, J. F.; Holland, E. K.; Fregoso, G. M.; Anthony, J. E.; Bronstein, H.; Friend, R.; Ryan, A. J.; Jones, R. A. L.; Greenham, N. C.; Rao, A. Ligand-Directed Self-Assembly of Organic–Semiconductor/Quantum-Dot Blend Films Enables Efficient Triplet Exciton-Photon Conversion. *J. Am. Chem. Soc.* **2024**, *146* (11), 7763–7770. <https://doi.org/10.1021/jacs.4c00125>.
- (33) Maiti, S.; Siebbeles, L. D. A. Developments and Challenges Involving Triplet Transfer across Organic/Inorganic Heterojunctions for Singlet Fission and Photon Upconversion. *J. Phys. Chem. Lett.* **2023**, *14* (49), 11168–11176. <https://doi.org/10.1021/acs.jpcclett.3c03013>.
- (34) Glaser, F.; Schmitz, M.; Kerzig, C. Coulomb Interactions for Mediator-Enhanced Sensitized Triplet–Triplet Annihilation Upconversion in Solution. *Nanoscale* **2024**, *16* (1), 123–137. <https://doi.org/10.1039/D3NR05265F>.
- (35) Cheng, Y. Y.; Nattestad, A.; Schulze, T. F.; MacQueen, R. W.; Fückel, B.; Lips, K.; Wallace, G. G.; Khoury, T.; Crossley, M. J.; Schmidt, T. W. Increased Upconversion Performance for Thin Film Solar Cells: A Trimolecular Composition. *Chem. Sci.* **2016**, *7* (1), 559–568. <https://doi.org/10.1039/C5SC03215F>.
- (36) Fückel, B.; Roberts, D. A.; Cheng, Y. Y.; Clady, R. G. C. R.; Piper, R. B.; Ekins-Daukes, N. J.; Crossley, M. J.; Schmidt, T. W. Singlet Oxygen Mediated Photochemical Upconversion of NIR Light. *J. Phys. Chem. Lett.* **2011**, *2* (9), 966–971. <https://doi.org/10.1021/jz200270w>.
- (37) Turshatov, A.; Busko, D.; Avlasevich, Y.; Miteva, T.; Landfester, K.; Balushev, S. Synergistic Effect in Triplet–Triplet Annihilation Upconversion: Highly Efficient Multi-Chromophore Emitter. *ChemPhysChem* **2012**, *13* (13), 3112–3115. <https://doi.org/10.1002/cphc.201200306>.
- (38) Cao, X.; Hu, B.; Zhang, P. High Upconversion Efficiency from Hetero Triplet–Triplet Annihilation in Multiacceptor Systems. *J. Phys. Chem. Lett.* **2013**, *4* (14), 2334–2338. <https://doi.org/10.1021/jz401213w>.
- (39) Schmidt, T. W.; Castellano, F. N. Photochemical Upconversion: The Primacy of Kinetics. *J. Phys. Chem. Lett.* **2014**, *5* (22), 4062–4072. <https://doi.org/10.1021/jz501799m>.
- (40) Raišys, S.; Juršėnas, S.; Simon, Y. C.; Weder, C.; Kazlauskas, K. Enhancement of Triplet-Sensitized Upconversion in Rigid Polymers via Singlet Exciton Sink Approach. *Chem. Sci.* **2018**, *9* (33), 6796–6802. <https://doi.org/10.1039/C8SC02151A>.
- (41) Radiunas, E.; Dapkevičius, M.; Raišys, S.; Juršėnas, S.; Jozeliūnaitė, A.; Javorskis, T.; Šinkevičiūtė, U.; Orentas, E.; Kazlauskas, K. Impact of T-Butyl Substitution in a Rubrene Emitter for Solid State NIR-to-Visible Photon Upconversion. *Phys. Chem. Chem. Phys.* **2020**, *22* (14), 7392–7403. <https://doi.org/10.1039/D0CP00144A>.

- (42) Wu, M.; Congreve, D. N.; Wilson, M. W. B.; Jean, J.; Geva, N.; Welborn, M.; Van Voorhis, T.; Bulović, V.; Bawendi, M. G.; Baldo, M. A. Solid-State Infrared-to-Visible Upconversion Sensitized by Colloidal Nanocrystals. *Nature Photonics* **2016**, *10* (1), 31–34. <https://doi.org/10.1038/nphoton.2015.226>.
- (43) Carrod, A. J.; Berghuis, A. M.; Gopalakrishnan, V. N.; Monkman, A.; Danos, A.; Börjesson, K. Separating Triplet Exciton Diffusion from Triplet–Triplet Annihilation by the Introduction of a Mediator. *Chem. Sci.* **2025**, *16* (3), 1293–1301. <https://doi.org/10.1039/D4SC07004F>.
- (44) Olesund, A.; Ghasemi, S.; Moth-Poulsen, K.; Albinsson, B. Bulky Substituents Promote Triplet–Triplet Annihilation Over Triplet Excimer Formation in Naphthalene Derivatives. *J. Am. Chem. Soc.* **2023**, *145* (40), 22168–22175. <https://doi.org/10.1021/jacs.3c08115>.
- (45) Olesund, A.; Johnsson, J.; Edhborg, F.; Ghasemi, S.; Moth-Poulsen, K.; Albinsson, B. Approaching the Spin-Statistical Limit in Visible-to-Ultraviolet Photon Upconversion. *J. Am. Chem. Soc.* **2022**, *144* (8), 3706–3716. <https://doi.org/10.1021/jacs.1c13222>.
- (46) Yamamoto, T.; Katsuta, H.; Toyota, K.; Iwamoto, T.; Morita, N. Preparation of 4,7-Dibromobenzo[b]Thiophene as a Versatile Building Block and Synthetic Application to a Bis(Ethynylthienyl)Oligoarene System. *Bulletin of the Chemical Society of Japan* **2012**, *85* (5), 613–623. <https://doi.org/10.1246/bcsj.20100345>.
- (47) Day, J. I.; Allen-Moyer, K. N.; Cole, K. P. Process Development for a 1H-Indazole Synthesis Using an Intramolecular Ullmann-Type Reaction. *J. Org. Chem.* **2023**, *88* (7), 4209–4223. <https://doi.org/10.1021/acs.joc.2c02771>.
- (48) Zähringer, T. J. B.; Moghtader, J. A.; Bertrams, M.-S.; Roy, B.; Uji, M.; Yanai, N.; Kerzig, C. Blue-to-UVB Upconversion, Solvent Sensitization and Challenging Bond Activation Enabled by a Benzene-Based Annihilator. *Angewandte Chemie International Edition* **2023**, *62* (8), e202215340. <https://doi.org/10.1002/anie.202215340>.
- (49) Gray, V.; Dzebo, D.; Lundin, A.; Alborzpour, J.; Abrahamsson, M.; Albinsson, B.; Moth-Poulsen, K. Photophysical Characterization of the 9,10-Disubstituted Anthracene Chromophore and Its Applications in Triplet–Triplet Annihilation Photon Upconversion. *J. Mater. Chem. C* **2015**, *3* (42), 11111–11121. <https://doi.org/10.1039/C5TC02626A>.
- (50) Kalpattu, A.; Dilbeck, T.; Hanson, K.; Fourkas, J. T. Extracting Accurate Information from Triplet–Triplet Annihilation Upconversion Data with a Mass-Conserving Kinetic Model. *Phys. Chem. Chem. Phys.* **2022**, *24* (46), 28174–28190. <https://doi.org/10.1039/D2CP03986A>.

Insert Table of Contents artwork here



Supporting Information for: Improving Triplet-Triple Annihilation Upconversion Output by a Triplet Mediator Approach: Mechanistic Insights on Homo and Hetero-Annihilation in Three Component Systems

Sunil Kumar Kandappa, Victor Gray*

Table of Contents

1. General Experimental details	11
2. Photophysical experiments	12
3. Synthesis	13
3.1. Synthesis of TIPS-Nap; 1,4-bis[2-[tris(1-methylethyl)silyl]ethynyl]naphthalene	13
3.2. Synthesis of TIPS-Ph; 1,4-bis[2-[tris(1-methylethyl)silyl]ethynyl]benzene	14
3.3. Synthesis of 3,6-dibromo-2-fluorobenzaldehyde.....	15
3.4. Synthesis of 3,6-dibromo-2-[(1,1-dimethylethyl)thio]benzaldehyde	15
3.5. Synthesis of tosyl azide.....	16
3.6. Synthesis of dimethyl (1-diazo-2-oxopropyl)phosphonate.....	16
3.7. Synthesis of 1,4-dibromo-2-[(1,1-dimethylethyl)thio]-3-ethynylbenzene	17
3.8. Synthesis of 4,7-dibromobenzo[<i>b</i>]thiophene	18
3.9. Synthesis of TIPS-BT; 4,7-bis[2-[tris(1-methylethyl)silyl]ethynyl]benzo[<i>b</i>]thiophene	18
4. TTA-UC quantum yield data	19
5. Plot of integrated area vs laser energy of upconverted emission intensity	20
6. UV-Vis absorption spectra of upconversion sample	24
7. Emission quantum yield determination of TIPS-BT	28
8. Stern-Volmer plot	30
9. NMR data.....	33
10. Kinetic Modelling.....	45
10.1. Figures from kinetic modelling.....	47
11. References.....	49

General Experimental details

All glassware was dried in an oven at 110 °C before reaction unless otherwise mentioned where dry glassware was not needed. All reactions were performed under argon atmosphere using standard Schlenk-line technique unless otherwise mentioned. For dry solvents, THF and toluene were collected from *Pure Solve MD7* solvent purification system and used as such without further drying.

All the chemicals are used as such received from vendors without further purification. NMR experiment performed with Jeol Eclipse+ 400 spectrometer for ^1H -400 MHz, ^{13}C -101MHz spectra at room temperature. The chemical shift values were reported in parts per million (PPM or δ) referenced to the residual solvent signal. For CDCl_3 it is 7.26 PPM for ^1H -NMR and 77.16 PPM for ^{13}C NMR.¹ NMR spectra of all compounds are recorded in CDCl_3 . The abbreviations s, singlet; d, doublet; t, triplet; q, quartet; m, multiplet; and brs, broad singlet used to describe multiplicities.

For high-resolution mass spectrometry (HRMS) experiments, the compounds were dissolved in acetonitrile (ACN) and mixed 1:1 with 2,5-dihydroxy benzoic acid (DHB) matrix solution (35mg/ml in 50% ACN/%0.01TFA) and 1 μl of mixed solution from each compound was spotted on MTP 384 ground steel target plates (Bruker Daltonics) and left for drying at room temperature. HR-MS experiments were performed in positive ionization mode using a matrix-assisted laser desorption/ionization Fourier-transform ion cyclotron resonance (MALDI-FTICR) (7T solariX XR-2 ω , Bruker Daltonics) mass spectrometer equipped with a Smartbeam II 2 kHz laser. The instrument was tuned for optimal detection of compounds (m/z 200–2000) in both polarities using the quadrature phase detection (QPD) (2 ω) mode and methods were calibrated externally with red phosphorus over an appropriate mass range for each compound analysis. Either M^+ or $[\text{M}+\text{H}]^+$ ions were detected for each compound and ppm errors were calculated. Molecular ion m/z values of each compound were calculated using Isotope pattern software (Bruker Daltonics). Molecular isotopic distributions of each molecule were also checked for validating the identity of the molecule.

Reactions were monitored by thin layer chromatography technique. Column chromatography techniques were used to isolate the product after the chemical reaction. Silica gel 200-400 mesh used for column chromatography. Freshly prepared lithium diisopropylamide solution² was used whenever required. The chemicals 1,4-dibromo-2-fluorobenzene, dimethyl(2-Oxopropyl)phosphonate, sodium-2-methyl-2-propanethiolate, CuI , PPh_3 , $\text{Pd}(\text{PPh}_3)_2\text{Cl}_2$, triisopropylsilylacetylene, DMF, tosyl chloride, sodium azide, and potassium carbonate were purchased from Sigma-Aldrich. Gold(I) chloride was purchased from abcr. For the synthesis involving TIPS-Nap, TIPS-BT and TIPS-Ph standard procedure³ of Sonogashira coupling was followed. TIPS-BT was synthesized by following the procedure reported earlier.⁴

Photophysical experiments

All the experiments involving triplet-triplet annihilation upconversion (TTA-UC) experiment were performed in deaerated toluene. Samples were prepared inside the glove box under argon atmosphere (with H_2O and O_2 level below 0.1 ppm). For all experiments involving TTA-UC and Stern-Volmer quenching same stock solution of sensitizer, annihilator and mediator was used to minimize the error associated with the sample preparation. Toluene was deaerated by using standard technique of freeze-pump-thaw (5 cycles). The solution of upconversion mixture was prepared inside the Glovebox in a cuvette with 4 mm path length in one side and 10 mm path length in the opposite side. For TTA-UC QY measurement, UV-Vis absorption was recorded through 4 mm and converted to the absorbance that correspond to 10 mm pathlength. For TTA-UC QY determination, sample was excited across 10 mm path of cuvette with emitted light detected in 90° angle, passing through the 4 mm path to minimize reabsorption of emitted light. For the UC QY determination, absorbance across 10 mm path length (excitation path) was considered. The steady state UV-visible absorption spectra were performed using Agilent Cary 50 spectrometer. Steady state fluorescence spectra and emission decay kinetics were recorded using FS5 Spectrofluorometer from Edinburgh Instruments. Upconversion experiments were performed using FLS1000 Photoluminescence Spectrometer from Edinburgh Instruments using an external 405 nm CW laser (MPN:X-III-405, 200 mW, Edinburgh Instruments) with a spot size of 12000 μm^2 . Upconversion quantum yield Φ_{UC} was determined by

the relative method^{5,6} using the standard compound Coumarin 153 in aerated ethanol ($\Phi_F = 0.53$) as per the equation-1, below. Here, A_r and A_{UC} absorbance of reference compound and upconversion sample at the excitation wavelength, F_{UC} and F_r are integrated emission intensity of upconversion sample and reference compound, η_r and η_{UC} are refractive index of solvent used for reference sample and upconversion sample respectively.

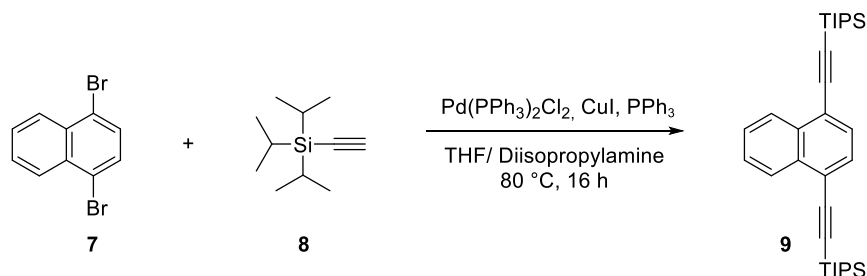
$$\Phi_{UC} = \Phi_r \left[\frac{A_{UC}}{A_r} \frac{F_{UC}}{F_r} \frac{\eta_r^2}{\eta_{UC}^2} \right] \dots \dots \dots (1)$$

TTA-UC QY values reported after relative method without any correction as well as with correction for reabsorption of emitted light by annihilator. Previously reported method⁷⁻⁹ was employed to correct for reabsorption where the fluorescence spectra of a dilute solution of annihilator is normalized to the upconverted emission spectra at a wavelength in the lower energy region of emission spectra with minimal reabsorption.

The flash-photolysis experiments were carried out using a Nd:YAG laser (Ekspla, NT342B laser) as the source of excitation of the samples with an OPO set at 410 nm having energies of 2 mJ/pulse. The spectrometer (LP920, Edinburgh Instruments) comprises a pulsed 450 W ozone-free Xe arc lamp, a symmetrical Czerny-Turner monochromator (TMS300) with 5 nm bandwidth and detectors for both single kinetic traces (LP900 photomultiplier, with Tektronix TDS3012C oscilloscope) and entire spectra (Andor SH720 ICCD camera).

Synthesis

Synthesis of TIPS-Nap; 1,4-bis[2-[tris(1-methylethyl)silyl]ethynyl]naphthalene



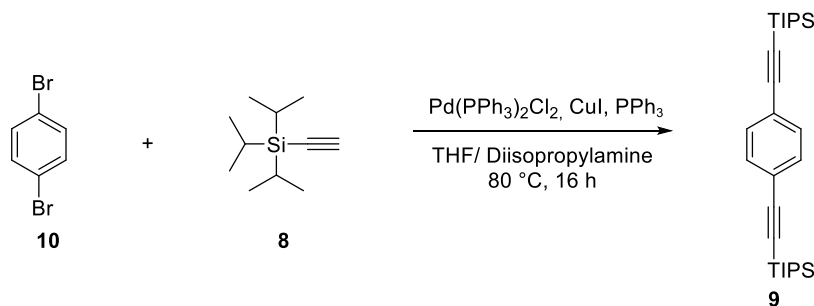
Procedure for this synthesis was adapted from the previous report³. A 250 mL two neck round bottomed flask was charged with 1, 4-dibromo naphthalene (1.44 g, 5.04 mmol, 1 equiv), CuI (60.5mg, 0.317 mmol, 0.06 equiv), PPh₃(1.44 mg, 0.317 mmol, 0.06 equiv) and Pd(PPh₃)₂Cl₂ (80.06 mg, 0.114 mmol, 0.02 equiv). The flask was purged with argon. Subsequently dry THF (40 mL) and diisopropyl amine (36 mL) was added under argon atmosphere. The reaction mixture was stirred at 80 °C for 5 minutes. The reaction mixture changed to orange colour. This was followed by the dropwise addition of triisopropylsilylacetylene under argon atmosphere (4.36 mL, 18.13 mmol, 3.6 equiv). It was further stirred at 80 °C for 16 h. Reaction was monitored by TLC. After the completion of reaction, the reaction mixture was cooled down to room temperature. Solvent was evaporated under reduced pressure in rotary evaporator. Crude material was dissolved in DCM (30 mL) and added DI water (30 mL). Organic layer separated and aqueous layer was further extracted with DCM (3 × 30 mL). Combined organic layer was dried with anhy. Na₂SO₄ and concentrated under reduced pressure. It was further purified by column chromatography.

Column chromatography: Crude material was adsorbed over ~ 5 mL of silica. Slurry of silica (100 mL) in heptane was loaded into a column. To the silica packed column, crude material adsorbed over silica was added. Column was further eluted with 400 mL of 100 % heptane. Eluent was collected as 25 mL fraction

in a test tube. Two sets of fractions were collected. First set of fractions from 9-12 had some nonpolar impurity as seen from TLC. Second set from 9-12 was pure by TLC. Impure fractions were combined and subjected to second column chromatography under the same condition mentioned above. Pure fractions from first and second column chromatography combined and concentrated to get pure product (2.12 g, yield = 88%).

Characterization: White solid, R_f : 0.8 in 100% heptane. ^1H NMR (400 MHz, CDCl_3): δ 8.39 (m, 2H), 7.65 – 7.57 (m, 4H), 1.19 (m, 42H). ^{13}C NMR (101 MHz, CDCl_3): δ 133.35, 130.29, 127.32, 126.76, 121.91, 104.89, 97.93, 18.92, 11.54. MALDI-HRMS m/z : Mass calculated for $[\text{M}^+]$ ion for $\text{C}_{32}\text{H}_{48}\text{Si}_2$; theoretical = 488.3295, Observed = 488.3284, $|\Delta\text{ppm}| = 2.2$ ppm.

Synthesis of TIPS-Ph; 1,4-bis[2-[tris(1-methylethyl)silyl]ethynyl]benzene

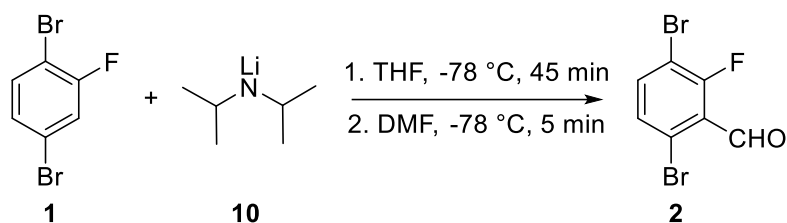


Procedure for this synthesis was adapted from previous report³. A 250 mL two neck round bottomed flask was charged with 1, 4-dibromo benzene (1.44 g, 6.10 mmol, 1 equiv), CuI (69.75 mg, 0.366 mmol, 0.06 equiv), PPh₃ (96 mg, 0.366 mmol, 0.06 equiv) and Pd(PPh₃)₂Cl₂ (86 mg, 0.122 mmol, 0.02 equiv). The mixture was purged with argon. Subsequently added dry THF (40 mL) and diisopropyl amine (36 mL) under argon atmosphere. The reaction mixture was stirred at 80 °C for 5 minutes. The reaction mixture changed to orange colour. Then added triisopropyl silylacetylide (5.28 mL, 21.97 mmol, 3.6 equiv) under argon atmosphere. It was further stirred at 80 °C for 16 h. Reaction was monitored by TLC. After the completion of reaction, the reaction mixture was cooled down to room temperature. Solvent was evaporated under reduced pressure in rotary evaporator. Crude material was dissolved in DCM (30 mL) and added DI water (30 mL). Organic layer separated and aqueous layer was further extracted with DCM (3 × 30 mL). Combined organic layer was dried with anhy. Na₂SO₄ and concentrated under reduced pressure. It was further purified by column chromatography.

Column chromatography: Crude material was adsorbed over ~ 5 mL of silica. Slurry of silica (100 mL) in pentane was loaded into a column. To the silica packed column, crude material adsorbed over silica was added. Column was further eluted with 400 mL of 100 % pentane. Eluent was collected as 25 mL fraction in a test tube. Fractions 8-20 had product along with nonpolar impurity. It was further subjected to the second column chromatography under the condition mentioned above to get pure product. (2.2 g, yield = 82%).

Characterization: White solid, R_f : 0.8 in 100% pentane. ^1H NMR (400 MHz, CDCl_3): δ 7.39 (s, 4H), 1.13 (s, 42H). ^{13}C NMR (101 MHz, CDCl_3): δ 131.92, 123.50, 106.78, 92.81, 18.81, 11.45. MALDI-HRMS m/z : Mass calculated for $[\text{M}^+]$ ion for $\text{C}_{32}\text{H}_{48}\text{Si}_2$; theoretical = 438.3138, Observed = 438.3131, $|\Delta\text{ppm}| = 1.6$ ppm.

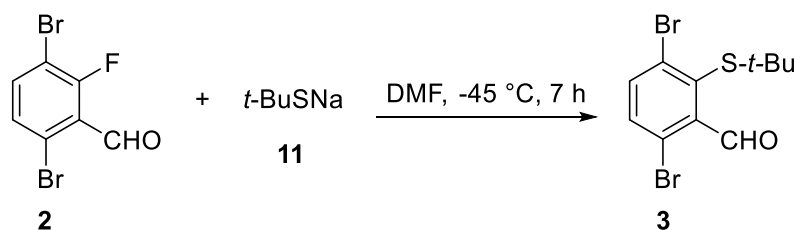
Synthesis of 3,6-dibromo-2-fluorobenzaldehyde



Procedure for this synthesis was adapted from previous report¹⁰. For the synthesis of aldehyde derivative freshly prepared LDA solution was prepared. For the preparation LDA solution, a 50 mL round bottomed flask was charged with 10 mL of dry THF and 2.5 mL of diisopropyl amine (freshly distilled over CaH₂). The mixture was cooled to -78 °C and added nBuLi (2.5 M in hexane). It was stirred for about a minute and used as such for the next step.

A 100 mL Schlenk flask was charged with 1,4-dibromo-2-fluoro benzene (4 g, 15,75 mmol, 1 equiv) and flushed with argon. Then added 40 mL of dry THF and the mixture was cooled to -78 °C in liq. N₂ / acetone bath. Subsequently added freshly prepared LDA solution (15,91 mL, 1 M, 15,91 mmol, 1.01 equiv) and stirred at the same temperature for 45 min. Afterwards DMF (3,05 mL, 39,39 mmol, 2.5 equiv) was added. The mixture was further stirred for 5 min and then quenched with 4 mL of DI water. The reaction mixture was allowed to warm to room temperature. Further 10 mL of DI water was added. Organic layer was separated and aqueous layer was extracted with ethyl acetate (3 × 20 mL). Combined organic layer washed with brine solution, dried with anhy. Na₂SO₄, followed by filtration and concentration under reduced pressure. To the mixture n-heptane was added and the slurry formed was cooled to -70 °C and solid formed was filtered. The filtrate obtained was further cooled to -77 °C and the solid material formed was again filtered. Filtered solid material (yellow, fluffy solid) was combined and used as such without further purification for the next step described below. (Crude mass = 4.3 g, crude yield = 96%).

Synthesis of 3,6-dibromo-2-[(1,1-dimethylethyl)thio]benzaldehyde



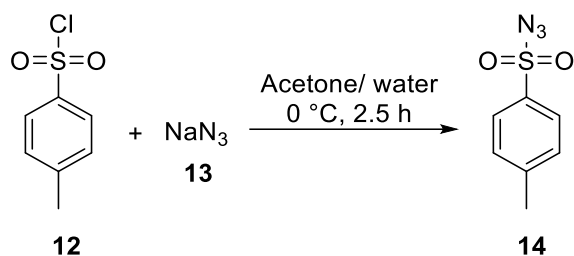
Procedure for this synthesis was adapted from previous report⁴. A 50 mL round bottomed flask was charged with 3,6 dibromo-2-fluorobenzaldehyde (4.0 g, 14,19 mmol, 1.0 equiv) and flushed with argon. Then added 20 mL of dry DMF. Another 100 mL Schlenk flask was charged with sodium-2-methyl-2-propanethiolate, *t*-BuSNa (1.75 g, 15.61 mmol, 1.1 equiv) and flushed with argon. Then added 12 mL of dry DMF and cooled to -45 °C (in acetonitrile/liq. N₂ mixture). To this mixture previously prepared solution of 3,6 dibromo-2-fluorobenzaldehyde in 20 mL of dry DMF was added at -45 °C. The reaction mixture was further stirred at the same temperature for 7 h. Reaction was monitored by TLC. Upon completion of reaction, it was poured into saturated solution of NH₄Cl (20 mL). Then added 10 mL of diethyl ether. Organic layer was separated. Aqueous layer was extracted with diethyl ether (3 × 20 mL). Combined organic layer was dried with anhy. Na₂SO₄ and concentrated under reduced pressure. It was further purified by column chromatography.

Column chromatography: Crude material was adsorbed over ~ 10 mL of silica. Slurry of silica (90 mL) in pentane was loaded into a column. To the silica packed column, crude material adsorbed over silica was added. Column was further eluted with 100% pentane and DCM/ pentane mixture. Eluent was collected as 25 mL fraction in a test tube. Following solvent mixtures were eluted.

300 mL of 100 % pentane, 200 mL of 2.5 % DCM/ pentane, 200 mL of 5 % DCM/ pentane, 200 mL of 10 % DCM/ pentane, 200 mL of 12.5 % DCM/ pentane, 200 mL of 15 % DCM/ pentane, 200 mL of 20 % DCM/ pentane. Clean fractions from 19-25 concentrated to get pure product. (4.0 g, yield = 80 %).

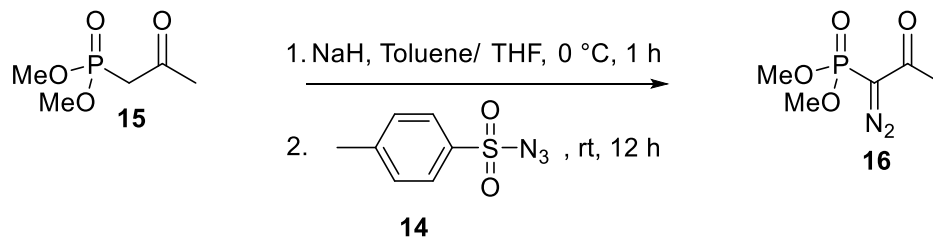
Characterization: Yellow solid, R_f : 0.4 in 20% DCM in pentane. ^1H NMR (400 MHz, CDCl_3): δ 7.39 (s, 4H), 1.13 (s, 42H). ^{13}C NMR (101 MHz, CDCl_3): δ 192.39, 143.53, 137.53, 136.82, 136.36, 134.63, 119.89, 52.71, 31.64. MALDI-HRMS m/z : Mass calculated for $[\text{M}^+]$ ion for $\text{C}_{32}\text{H}_{48}\text{Si}_2$; theoretical = 349.8976, Observed = 349.8972, $|\Delta\text{ppm}| = 1.1$ PPM.

Synthesis of tosyl azide



Procedure for this synthesis was adapted from previous report¹¹. A 100 mL round bottomed flask was charged with 4 g of tosyl chloride. Then added 25 mL of acetone and 25 mL of water. The mixture was cooled to 0 °C in an ice bath. Subsequently added sodium azide portion wise. It was further stirred at the same temperature for 2.5 h. The reaction mixture was concentrated to the half of initial volume under reduced pressure. Then added 20 mL of diethyl ether. Organic layer was separated and the aqueous layer was extracted with diethyl ether (3 × 20 mL). Combined organic layer was dried with anhydrous Na_2SO_4 and concentrated under reduced pressure in rotary evaporator with maintaining the temperature of water bath at room temperature. Crude material (pale yellow solid) was taken as such for the next step described below. (Crude mass = 4.0 g, crude yield = 96%).

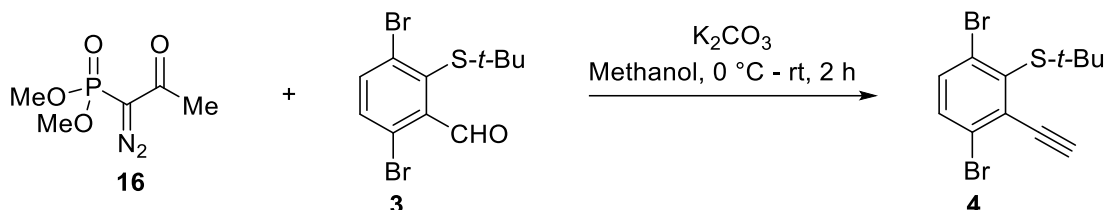
Synthesis of dimethyl (1-diazo-2-oxopropyl)phosphonate



Procedure for this synthesis was adapted from previous report¹². A 100 mL Schlenk flask was charged with NaH (722 mg, 60% dispersion in mineral oil, 18.06 mmol, 1.5 equiv). Then added 25 mL of toluene and 7 mL of THF. The mixture was cooled to 0 °C. Subsequently dimethyl acetylmethylphosphonate (2 g, 12.04 mmol, 1 equiv) was added to the mixture at the same temperature. The mixture was stirred for 1 h at 0

°C. Afterwards tosyl azide (2.37 g, 12.04 mmol, 1 equiv) was added and the mixture was further stirred for 12 h at rt. Then the mixture was filtered over Celite pad and the filtrate was concentrated under reduced pressure in rotary evaporator with maintaining the temperature of water bath at room temperature. Crude material (orange oily liquid) was taken as such for the next step described below. (Crude mass = 2.3 g, crude yield = 99%).

Synthesis of 1,4-dibromo-2-[(1,1-dimethylethyl)thio]-3-ethynylbenzene



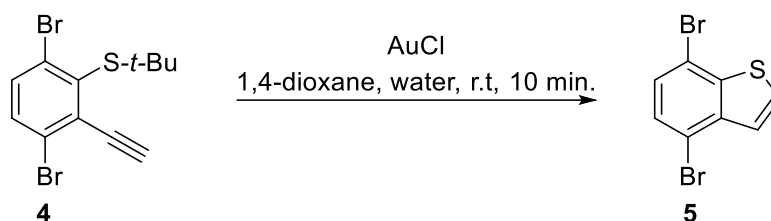
Procedure for this synthesis was adapted from previous report⁴. A 100 mL round bottomed flask was charged with aldehyde derivative (4.57 g, 12.98 mmol, 1.2 equiv) and added 50 mL of methanol. Aldehyde derivative was made sure to dissolve completely in methanol. Another 250 mL Schlenk flask was charged with dimethyl acetylmethylphosphonate (4.99 g, 25.96 mmol, 2 equiv) and added 60 mL of methanol. Subsequently added potassium carbonate (5.38 g, 38.93 mmol, 3 equiv) and the mixture was cooled to 0 °C in ice bath. To this mixture, previously prepared solution of aldehyde derivative in 50 mL of methanol was added at 0 °C. The mixture was allowed to warm to rt. and stirred at the same temperature for 2 h. Reaction was monitored by TLC. Upon completion of reaction the mixture was poured into DI water (20 mL) and added 20 mL of DI water. Organic layer was separated and aqueous layer was extracted with diethyl ether (3x 10 mL). Combined organic layer was washed with brine solution and dried over anhy. Na₂SO₄. It was concentrated under reduced pressure in rotary evaporator and purified by column chromatography.

Column chromatography: Crude material was adsorbed over ~ 10 mL of silica. Slurry of silica (200 mL) in pentane was loaded into a column. To the silica packed column, crude material adsorbed over silica was added. Column was further eluted with 100% pentane and DCM/ pentane mixture. Eluent was collected as 25 mL fraction in a test tube. Following solvent mixtures were eluted.

100 mL of 100 % pentane, 200 mL of 2.5 % DCM/ pentane, 200 mL of 5 % DCM/ pentane, 200 mL of 7.5 % DCM/ pentane, 200 mL of 10 % DCM/ pentane, 200 mL of 12.5 % DCM/ pentane, 200 mL of 15 % DCM/ pentane and 200 mL of 17.5% DCM/ pentane. Clean fractions from 16-36 concentrated to get pure product. (3.4 g, yield = 75 %).

Characterization: White solid, R_f: 0.8 in 20% DCM in pentane. ¹H NMR (400 MHz, CDCl₃): δ 7.54 (d, J = 8.6 Hz, 1H), 7.45 (d, J = 8.7 Hz, 1H), 3.65 (s, 1H), 1.42 (s, 10H). ¹³C NMR (101 MHz, CDCl₃): δ 138.93, 134.06, 134.02, 133.92, 133.59, 126.13, 87.27, 82.72, 53.06, 32.00. MALDI-HRMS *m/z*: Mass calculated for [M⁺] ion for C₃₂H₄₈Si₂; theoretical = 345.9026, Observed = 345.9021, |Δppm| = 1.4 ppm.

Synthesis of 4,7-dibromobenzo[*b*]thiophene

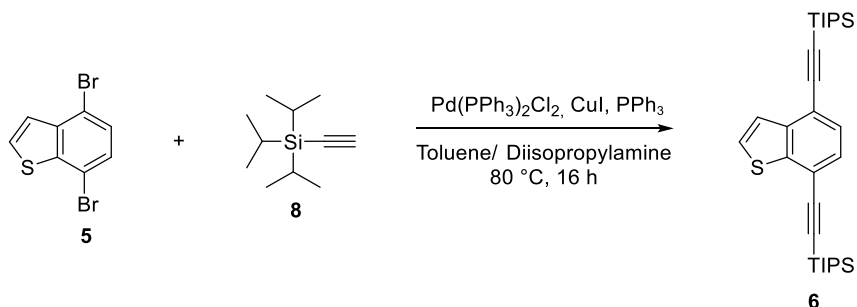


Procedure for this synthesis was adapted from previous report.⁴ A 100 mL round bottomed flask was charged with dibromo thiol derivative (3.38 g, 9.71 mmol, 1 equiv). Then added 1,4-dioxane (30 mL) and DI water (6 mL). Subsequently added gold chloride, AuCl (90.27 mg, 0.3884 mmol). The reaction mixture was stirred at rt for 10 min. Reaction was monitored by TLC. Upon completion of reaction solvent was evaporated in rotary evaporator and the crude material was purified by column chromatography.

Column chromatography: Crude material was adsorbed over ~ 10 mL of silica. Slurry of silica (100 mL) in pentane was loaded into a column. To the silica packed column, crude material adsorbed over silica was added. Column was further eluted with 600 mL of 100% pentane. Clean fractions from 9-19 concentrated to get pure product. (2.6 g, yield = 92 %).

Characterization: White solid, R_f : 0.8 in 100% pentane. ^1H NMR (400 MHz, CDCl_3): δ 7.62 – 7.54 (m, 2H), 7.43 (d, $J = 8.1$ Hz, 1H), 7.35 (d, $J = 8.1$ Hz, 1H). ^{13}C NMR (101 MHz, CDCl_3): δ 142.34, 140.21, 128.79, 128.39, 128.04, 125.55, 116.53, 115.04. MALDI-HRMS m/z : Mass calculated for $[\text{M}^+]$ ion for $\text{C}_{32}\text{H}_{48}\text{Si}_2$; theoretical = 289.8400, Observed = 289.8394, $|\Delta\text{ppm}| = 2.1$ ppm.

Synthesis of TIPS-BT; 4,7-bis[2-[tris(1-methylethyl)silyl]ethynyl]benzo[*b*]thiophene



Procedure for this synthesis was adapted from previous report.³ A 100 mL Schlenk flask was charged with 1, 4-dibromo naphthalene (1.48 g, 5.07 mmol, 1 equiv), CuI (57.92 mg, 0.304 mmol, 0.06 equiv), PPh_3 (79.7 mg, 0.304 mmol, 0.06 equiv) and $\text{Pd}(\text{PPh}_3)_2\text{Cl}_2$ (71.15 mg, 0.101 mmol, 0.02 equiv). The flask was purged with argon. Subsequently dry toluene (60 mL) and diisopropyl amine (18 mL) was added under argon atmosphere. The reaction mixture was stirred at 80 °C for 5 minutes. The reaction mixture changed to orange colour. This was followed by the dropwise addition of triisopropyl silyl acetylide under argon atmosphere (2.68 mL, 11.15 mmol, 2.2 equiv). It was further stirred at 80 °C for 16 h. Reaction was monitored by TLC. After the completion of reaction, the reaction mixture was cooled down to room temperature. Solvent was evaporated under reduced pressure in rotary evaporator. Crude material was dissolved in ethyl acetate (20 mL) and added DI water (20 mL). Organic layer separated and aqueous layer was further extracted with ethyl acetate (3 × 20 mL). Combined organic layer was dried with anhy. Na_2SO_4

and concentrated under reduced pressure in rotary evaporator. It was further purified by column chromatography.

Column chromatography: Crude material was adsorbed over ~ 10 mL of silica. Slurry of silica (125 mL) in pentane was loaded into a column. To the silica packed column, crude material adsorbed over silica was added. Column was further eluted with 600 mL of 100 % pentane. Eluent was collected as 25 mL fraction in a test tube. Fractions from 4-12 had product along with nonpolar impurity as seen from TLC. Impure fractions were combined and subjected to second column chromatography.

Crude material was adsorbed over ~ 10 mL of silica. Slurry of silica (350 mL) in pentane was loaded into a column. To the silica packed column, crude material adsorbed over silica was added. Column was further eluted with 900 mL of 100 % pentane. Eluent was collected as 25 mL fraction in a test tube. Fractions from 14-32 had product along with nonpolar impurity as seen from TLC. Impure fractions were combined and subjected to third column chromatography.

Crude material was adsorbed over ~ 10 mL of silica. Slurry of silica (500 mL) in pentane was loaded into a column. To the silica packed column, crude material adsorbed over silica was added. Column was further eluted with 900 mL of 100 % pentane. Pure fractions from 21-40 concentrated to get pure product (2.4 g, yield = 95%).

Characterization: White solid, R_f : 0.7 in 100% pentane. ^1H NMR (400 MHz, CDCl_3): δ 7.61 – 7.49 (m, 2H), 7.49 – 7.35 (m, 2H), 1.18 (d, $J = 3.4$ Hz, 42H). ^{13}C NMR (101 MHz, CDCl_3): δ 140.86, 128.35, 127.93, 127.39, 124.19, 118.65, 118.18, 105.03, 104.26, 97.85, 96.33, 18.88, 18.84, 11.51, 11.47, 11.43. MALDI-HRMS m/z : Mass calculated for $[\text{M}^+]$ ion for $\text{C}_{32}\text{H}_{48}\text{Si}_2$; theoretical = 494.2859, Observed = 494.2850, $|\Delta\text{ppm}| = 1.8$ ppm.

TTA-UC quantum yield data

Table S1: TTA UC QY before and after reabsorption correction for different upconversion samples in deaerated toluene.

Entry ^a	Upconversion system	TTA UC QY (%)	
		With reabsorption corrections ^c	No reabsorption corrections ^c
1	25 μM 4CzBN + 1mM Nap ^d	12.6 \pm 0.3	6.05 \pm 0.5
2	25 μM 4CzBN + 1mM Nap (10 mm cuvette) ^b	11.1 \pm 0.05	4.92 \pm 0.01
3	25 μM 4CzBN + 0.1 mM Nap + 1mM BT ^d	12.2 \pm 0.3	7.2 \pm 0.3
4	25 μM 4CzBN + 0.1 mM Nap	3.38 \pm 0.01	2.0 \pm 0.05
5	25 μM 4CzBN + 0.01 mM Nap + 1mM BT	7.8 \pm 0.15	5.4 \pm 0.1
6	25 μM 4CzBN + 0.01 mM Nap	0.2 \pm 0.02	0.15 \pm 0.02
7	25 μM 4CzBN + 1 mM BT	1.5 \pm 0.05	1.0 \pm 0.1

8	25 μ M 4CzBN + 10 mM BT	1.45 \pm 0.01	0.78 \pm 0.005
9	25 μ M 4CzBN + 0.1 mM Nap + 10mM BT	12.5 \pm 0.55	6.7 \pm 0.3
10	25 μ M 4CzBN + 0.1 mM Nap + 1 mM Ph	5.1 \pm 0.3	3.0 \pm 0.2

^aEntry 1, 3-10, TTA-UC QY was measured in 4 mm \times 10 mm cuvette, where sample was excited across 10 mm path of cuvette, with emitted light detected in 90° angle, passing through the 4 mm path to minimize reabsorption of emitted light. ^bEntry 2, TTA-UC QY was measured in 10 mm \times 10 mm cuvette to compare with that of 4 mm \times 10 mm cuvette for one sample (4CzBN + 1mM Nap). ^cAveraged over two trials except for entry 1 and 3. ^dAveraged over four trials with standard deviation as error. TIPS-Nap, TIPS-BT and TIPS-Ph are abbreviated as Nap, BT and Ph respectively.

Plot of integrated area vs laser energy of upconverted emission intensity

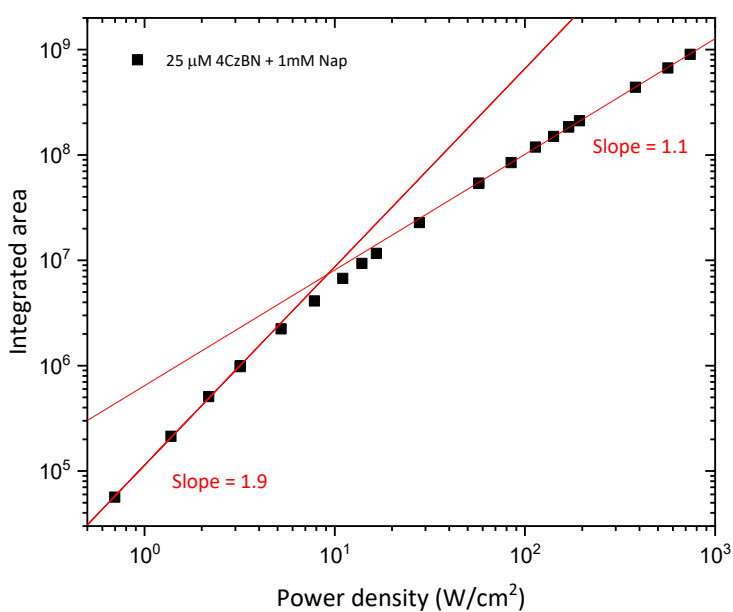


Figure S1: Laser power density vs integrated area of upconverted emission intensity for 25 mM 4CzBN + 1mM Nap.

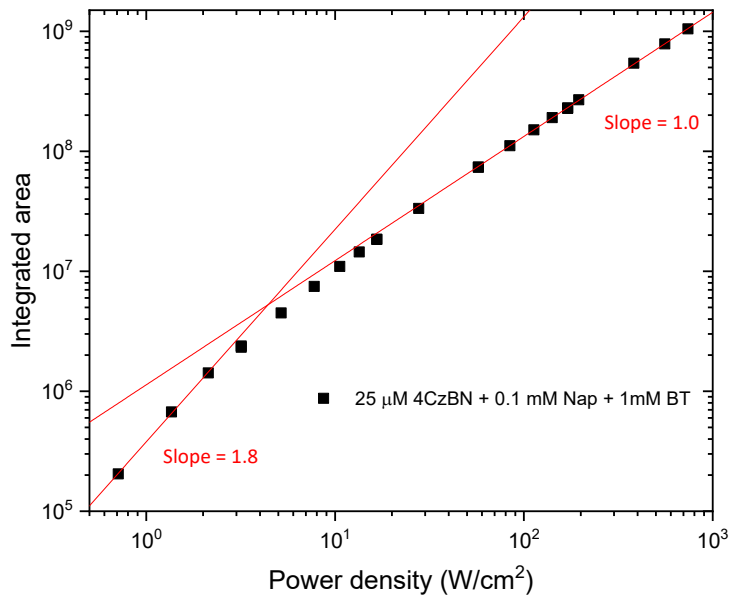


Figure S2: Plot of integrated area of upconverted emission intensity vs laser power density for 25 μM 4CzBN + 0.1 mM Nap + 1mM BT.

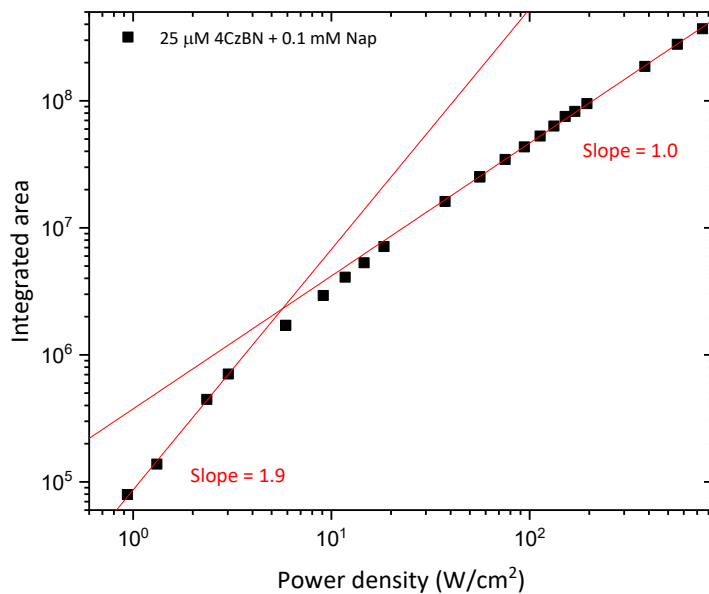


Figure S3: Plot of integrated area of upconverted emission intensity vs laser power density for 25 μM 4CzBN + 0.1 mM Nap.

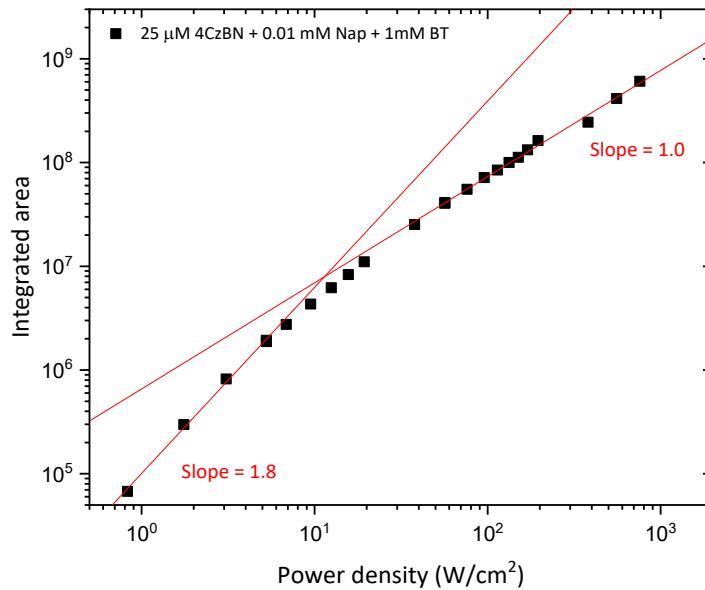


Figure S4: Plot of integrated area of upconverted emission intensity vs laser power density for 25 μM 4CzBN + 0.01 mM Nap + 1mM BT.

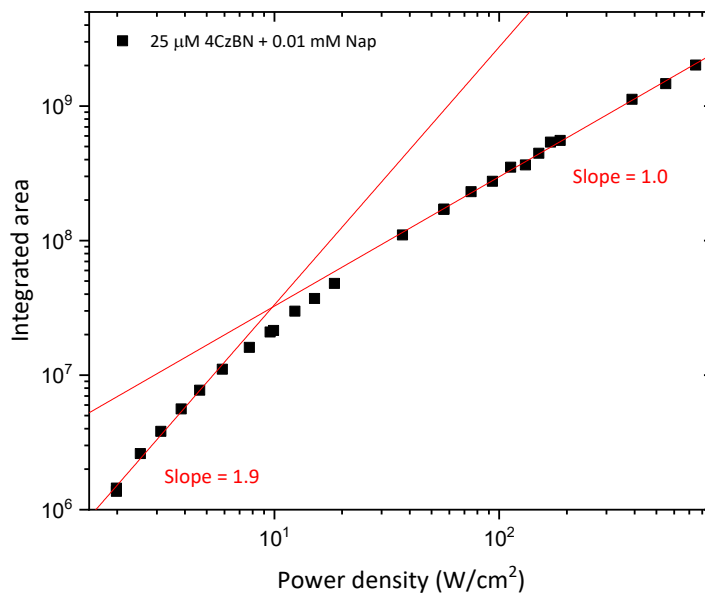


Figure S5: Plot of integrated area of upconverted emission intensity vs laser power density for 25 μM 4CzBN + 0.01 mM Nap.

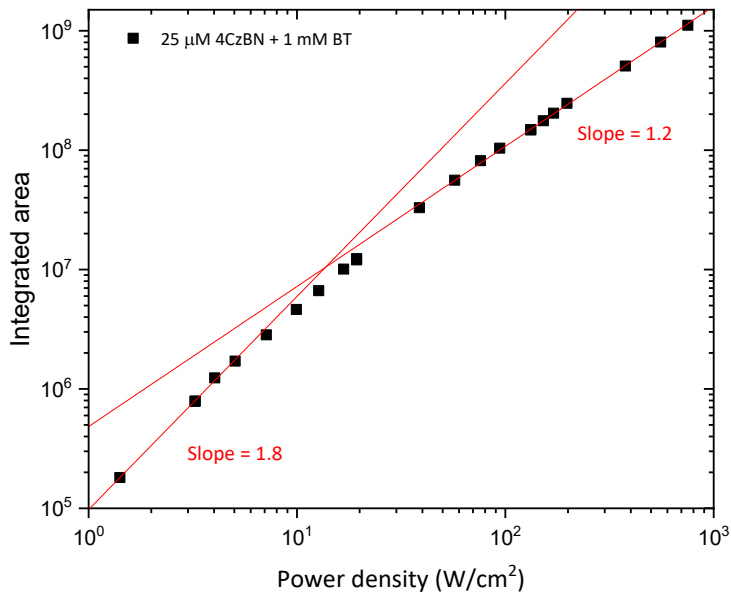


Figure S6: Plot of integrated area of upconverted emission intensity vs laser power density for 25 μM 4CzBN + 1 mM BT.

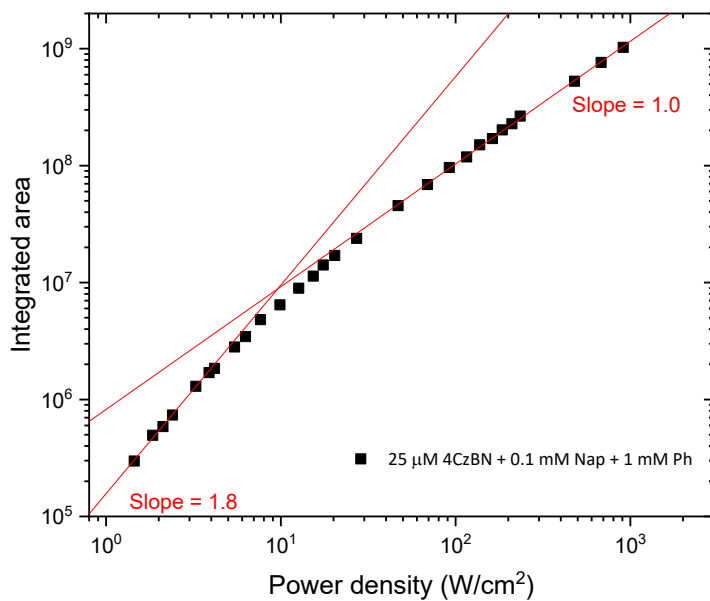


Figure S7: Plot of integrated area of upconverted emission intensity vs laser power density for 25 μM 4CzBN + 0.1 mM Nap + 1 mM Ph.

Table S2: I_{th} value and slope in the plot of laser energy vs integrated area of emission intensity of different upconversion samples in deaerated toluene.^a

Entry	Upconversion system	Slope in low intensity region	Slope in high intensity region	I_{th} value (W/cm ²)
1	25 μ M 4CzBN + 1mM Nap	1.9	1.1	9.2
2	25 μ M 4CzBN + 0.1 mM Nap + 1mM BT	1.8	1.0	4.4
3	25 μ M 4CzBN + 0.1 mM Nap	1.9	1.1	5.7
4	25 μ M 4CzBN + 0.01 mM Nap + 1mM BT	1.8	1.0	11.4
5	25 μ M 4CzBN + 0.01 mM Nap	1.9	1.0	9.8
6	25 μ M 4CzBN + 1 mM BT	1.8	1.2	13.7
7	25 μ M 4CzBN + 0.1 mM Nap + 1 mM Ph	2.1	1.1	4.0

^aTTA-UC emission was measured in 10 mm \times 10 mm cuvette. Laser energy was varied from high to low energy for each measurement. TIPS-Nap, TIPS-BT and TIPS-Ph are abbreviated as Nap, BT, and Ph respectively. The straight line obtained after fitting the data in the slope 1 and slope 2 region of integrated area vs power density plot was used to determine I_{th} value. Intersection point was determined after solving the equation for straight line.

UV-Vis absorption spectra of upconversion sample

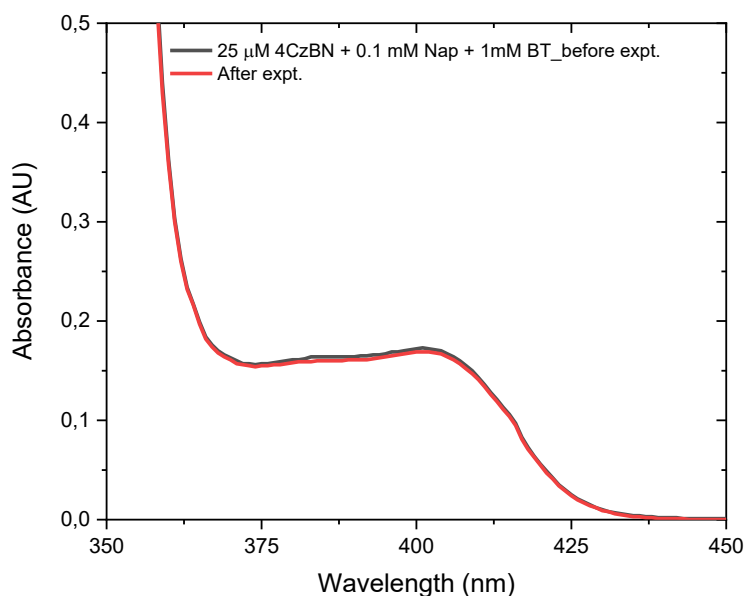


Figure S8: UV-Vis absorption spectra of 25 μ M 4CzBN + 0.1 mM Nap + 1mM BT before and after laser excitation in the experiment for the determination I_{th} value.

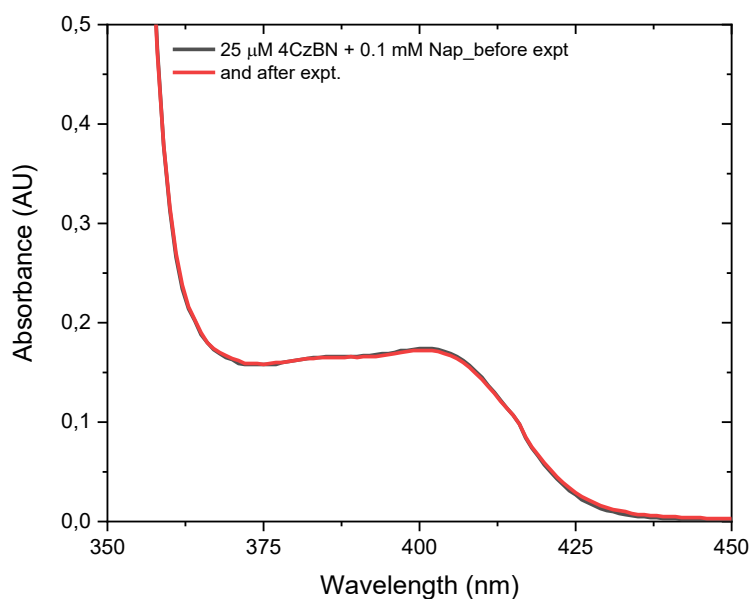


Figure S9: UV-Vis absorption spectra of 25 μM 4CzBN + 0.1 mM Nap before and after laser excitation in the experiment for the determination I_{th} value.

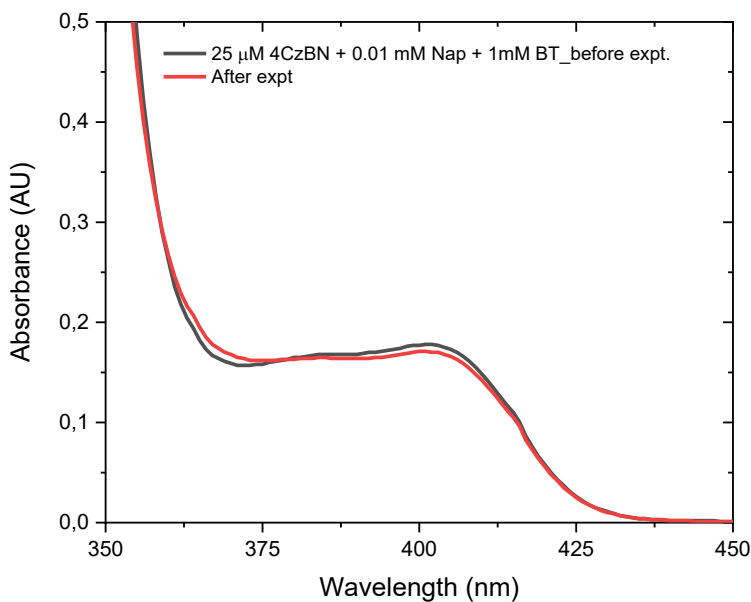


Figure S10: UV-Vis absorption spectra of 25 μM 4CzBN + 0.01 mM Nap + 1mM BT before and after laser excitation in the experiment for the determination I_{th} value.

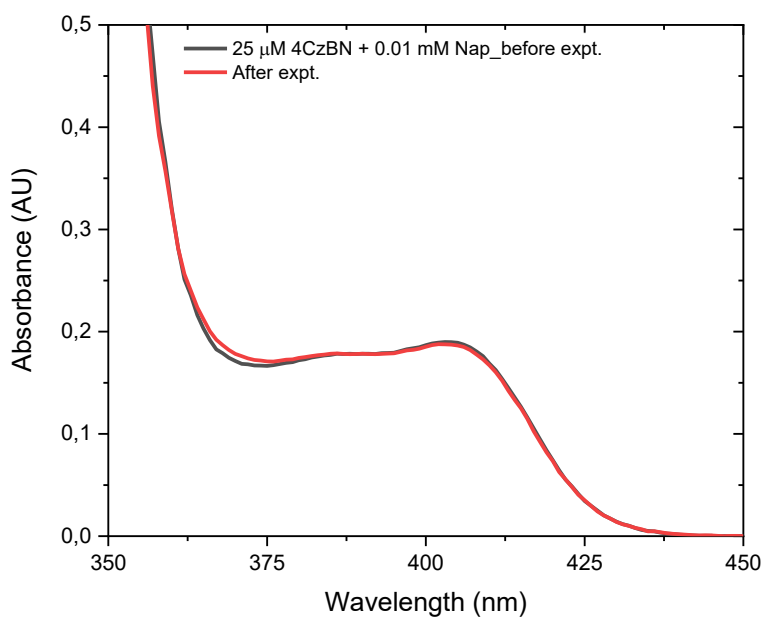


Figure S11: UV-Vis absorption spectra of 25 μM 4CzBN + 0.01 mM Nap before and after laser excitation in the experiment for the determination I_{th} value.

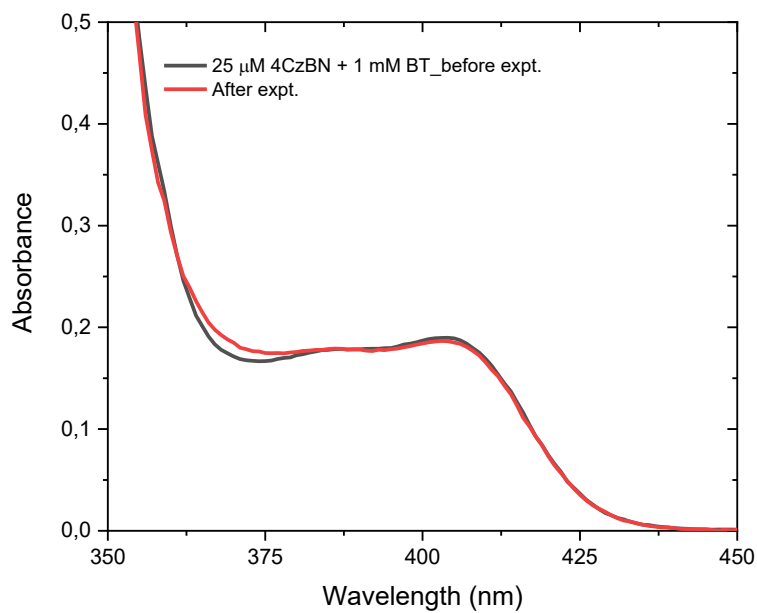


Figure S12: UV-Vis absorption spectra of 25 μM 4CzBN + 1 mM BT before and after laser excitation in the experiment for the determination I_{th} value.

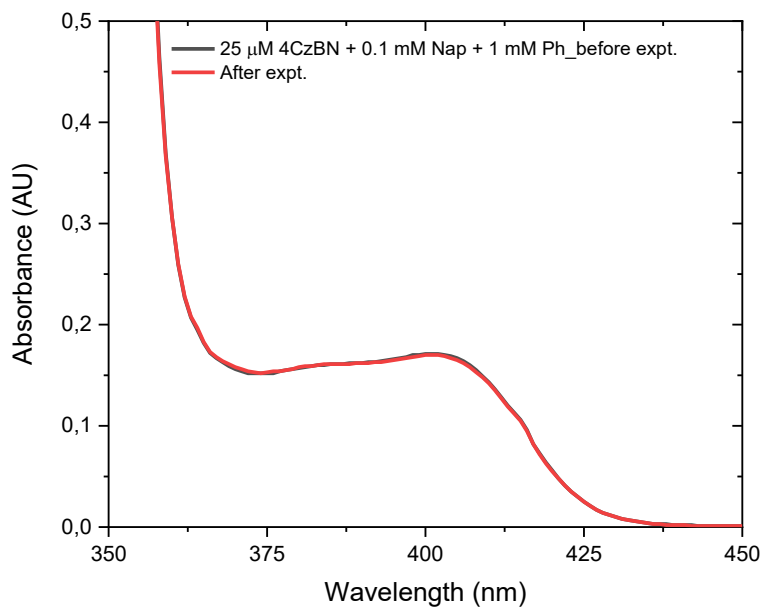


Figure S13: UV-Vis absorption spectra of 25 μM 4CzBN + 0.1 mM Nap + 1 mM Ph before and after laser excitation in the experiment for the determination I_{th} value.

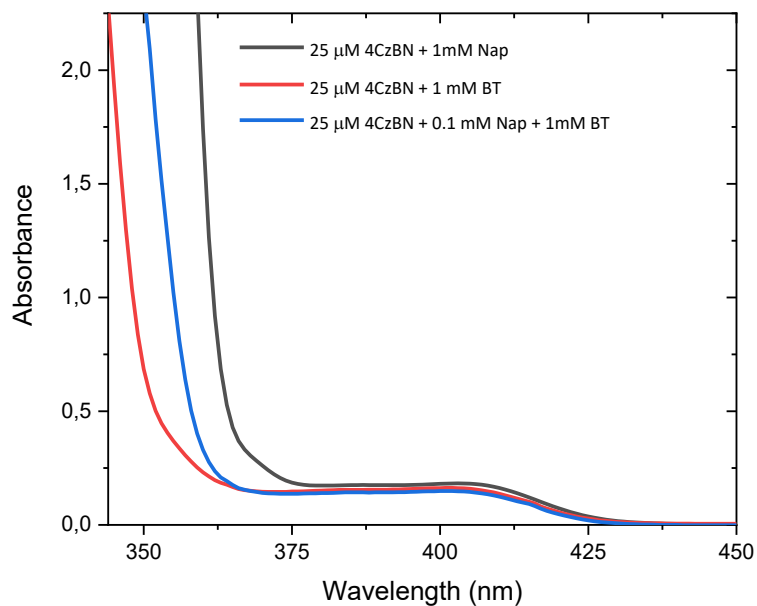


Figure S14: Comparison of UV-Vis absorption spectra of upconversion sample 25 μM 4CzBN + 0.1 mM Nap + 1mM BT with that of 25 μM 4CzBN + 1mM Nap and 25 μM 4CzBN + 1 mM BT.

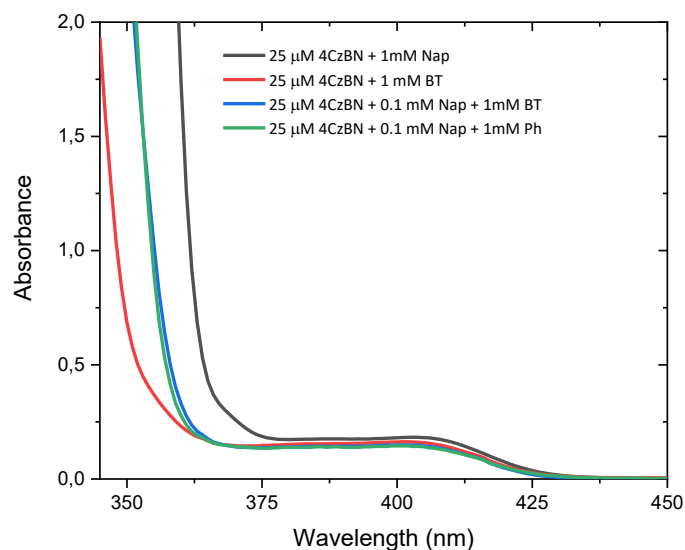


Figure S15: Comparison of UV-Vis absorption spectra of upconversion sample 25 μM 4CzBN + 0.1 mM Nap + 1mM Ph with that of 25 μM 4CzBN + 1mM Nap, 25 μM 4CzBN + 0.1 mM Nap + 1mM BT and 25 μM 4CzBN + 1 mM BT.

Emission quantum yield determination of TIPS-BT

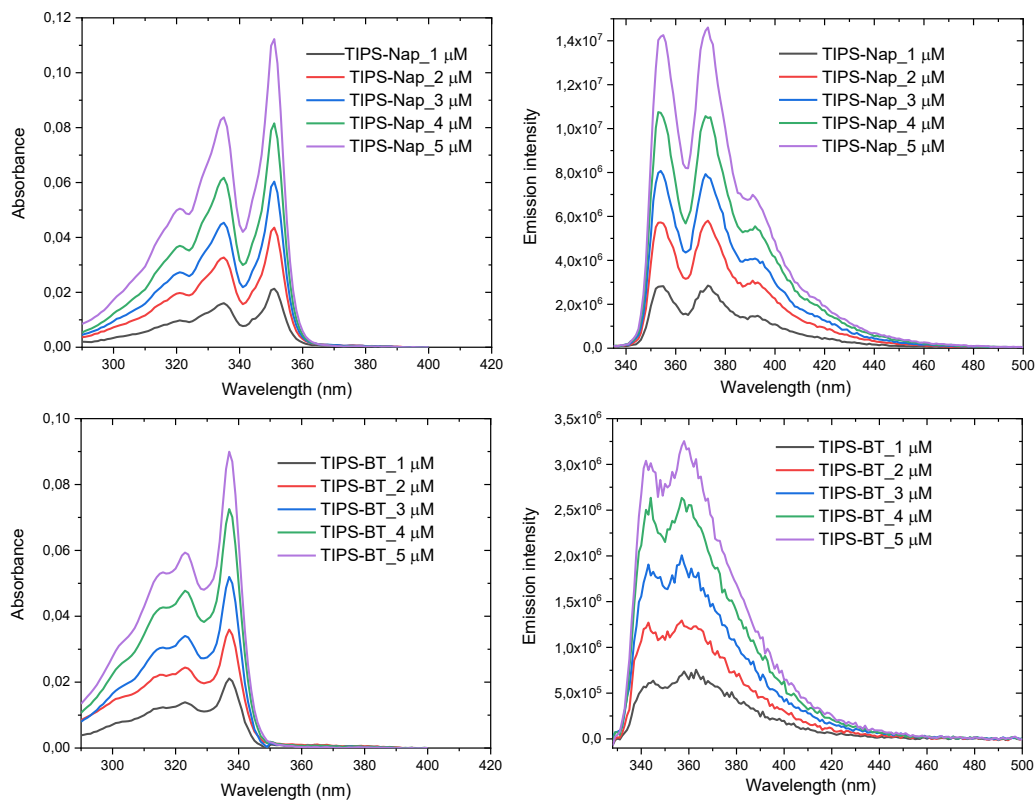


Figure S16: UV-Vis absorption (top left and bottom left) and emission (top right and bottom right) spectra of dilute solution of TIPS-Nap and TIPS-BT in toluene. Concentration ranges from 1-5 μM .

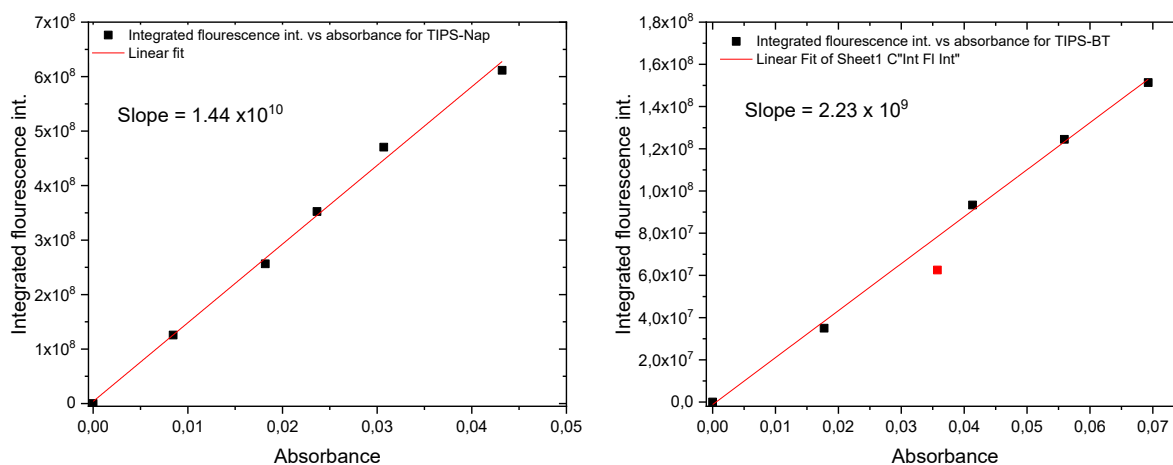


Figure S17: Plot of integrated fluorescence intensity vs absorbance for TIPS-Nap and TIPS-BT.

Fluorescence emission quantum yield of TIPS-BT determined using TIPS-Nap as reference in degassed toluene. The fluorescence quantum yield of TIPS-Nap = 0.77 adopted from the previous report.¹³ Following equation^{5,6} was considered to determine relative quantum yield of TIPS-BT with reference to TIPS-Nap. Abbreviation BT and Nap in the equation refers to TIPS-BT and TIPS-Nap.

To minimize the error associated with the quantum yield determination such as self-quenching, multiple trials are performed in the low concentration regime (with concentration 1-5 μM) (Figure 18). Same excitation wavelength and excitation, emission slit width maintained for the reference and sample emission. Plot of integrated emission intensity vs absorbance showed linear relationship as in figure 19.

Further parameters in equation 2 replaced with the slope of these plots as in equation 3 to determine fluorescence quantum yield. From this experiment, emission quantum yield of TIPS-BT was determined to be 11.9%.

$$\Phi_{BT} = \Phi_{Nap} \left[\frac{A_{Nap}}{A_{BT}} \times \frac{F_{BT}}{F_{Nap}} \times \frac{\eta_{BT}^2}{\eta_{Nap}^2} \right] \dots \dots \dots (2)$$

Or

$$\Phi_{BT} = \Phi_{Nap} \left[\frac{\text{Slope}_{BT}}{\text{Slope}_{Nap}} \times \frac{\eta_{Nap}^2}{\eta_{BT}^2} \right] \dots \dots \dots (3)$$

Stern-Volmer plot

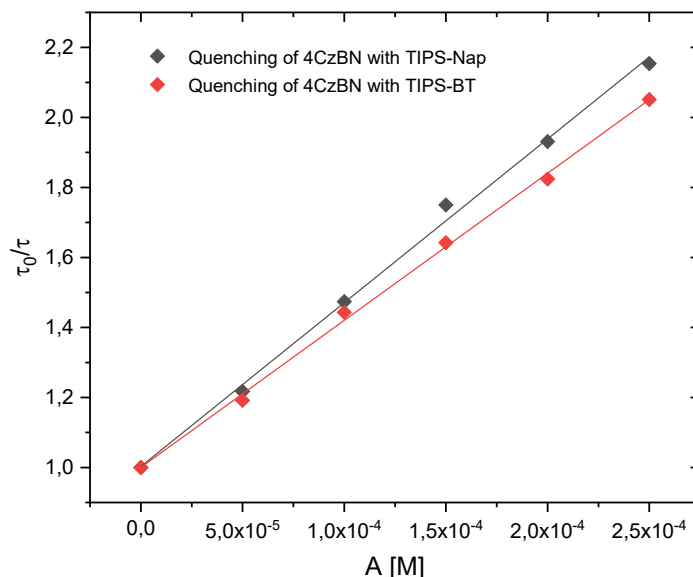


Figure S18: Stern-Volmer plot for the quenching of 4CzBN delayed lifetime with TIPS-BT and TIPS-Nap.

For Stern-Volmer plot, quenching of delayed fluorescence component of 4CzBN (since it exhibits TADF behaviour) was considered as reported elsewhere.¹³ Quenching experiment was performed in degassed toluene with 25 μM solution of 4CzBN and quencher concentration ranging from 0.05 mM to 0.25 mM was added. Rate constant for triplet energy transfer k_{TET} for TIPS-BT was found to be $0.75 \times 10^9 \text{ M}^{-1}\text{s}^{-1}$ slightly lower than that of TIPS-Nap which was $0.84 \times 10^9 \text{ M}^{-1}\text{s}^{-1}$. Under our experimental condition lifetime of delayed fluorescence of 4CzBN was found to be 5.6 μs .

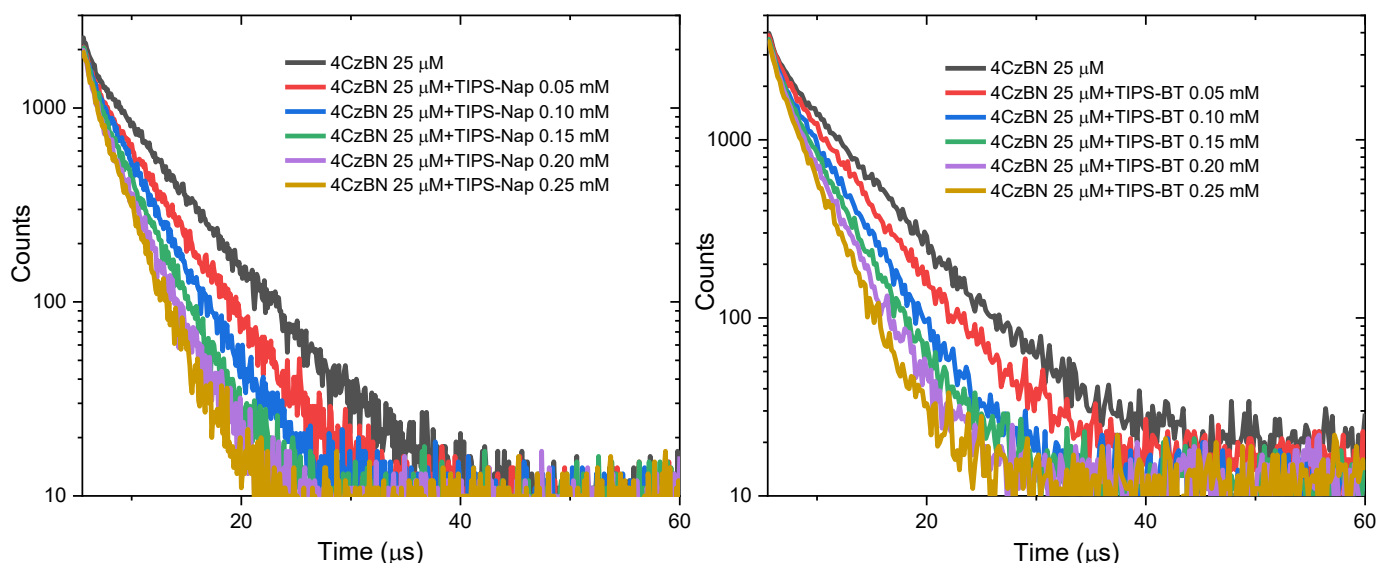


Figure S19: Decay trace of 4CzBN emission upon addition of TIPS-Nap and TIPS-BT. Excitation source = MCS laser diode. $\lambda_{\text{ex}} = 375 \text{ nm}$ and emission monitored at 500 nm. Em BW = 10 nm.

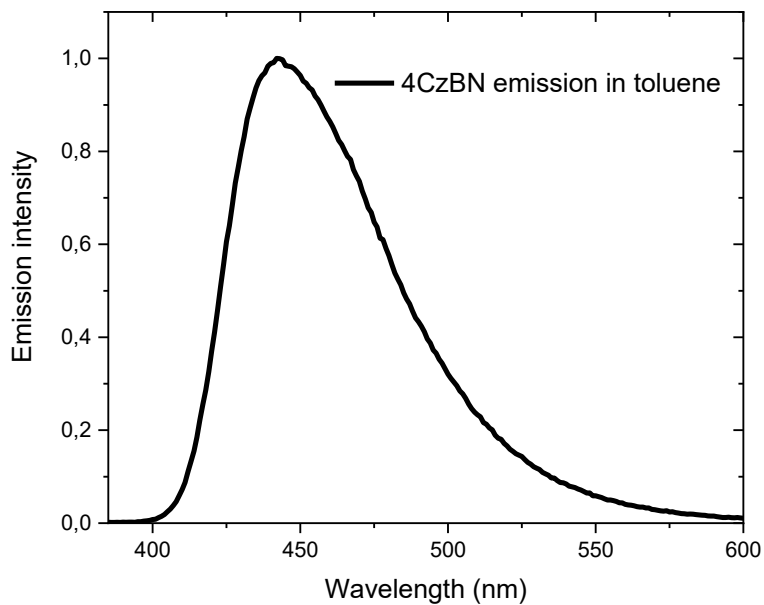


Figure S20: 4CzBN emission spectra in toluene (50 μM). Excitation source = Xe lamp. $\lambda_{\text{ex}} = 372 \text{ nm}$, Ex BW= 3 nm, Em BW = 5 nm.

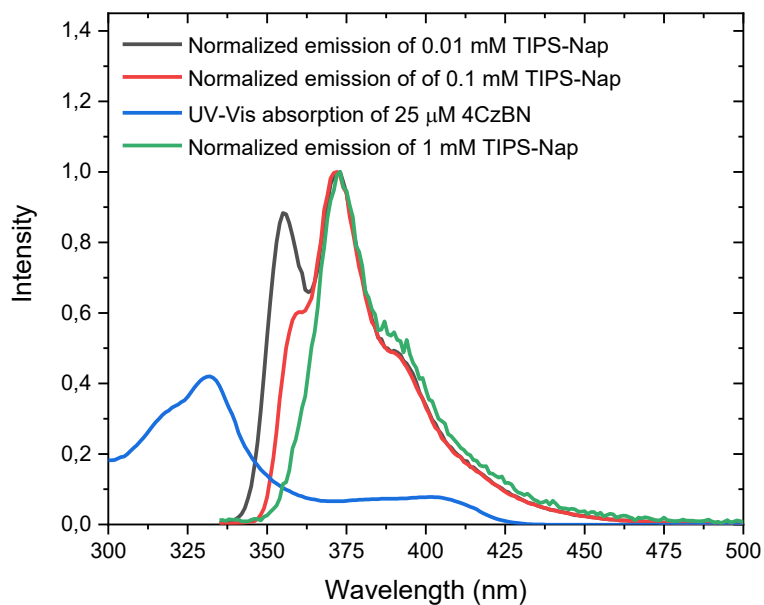


Figure S21: UV-Vis absorption spectra of 25 μM 4CzBN and normalized emission spectra of TIPS-Nap (1 mM, 0.1 mM and 0.01 mM) in toluene.

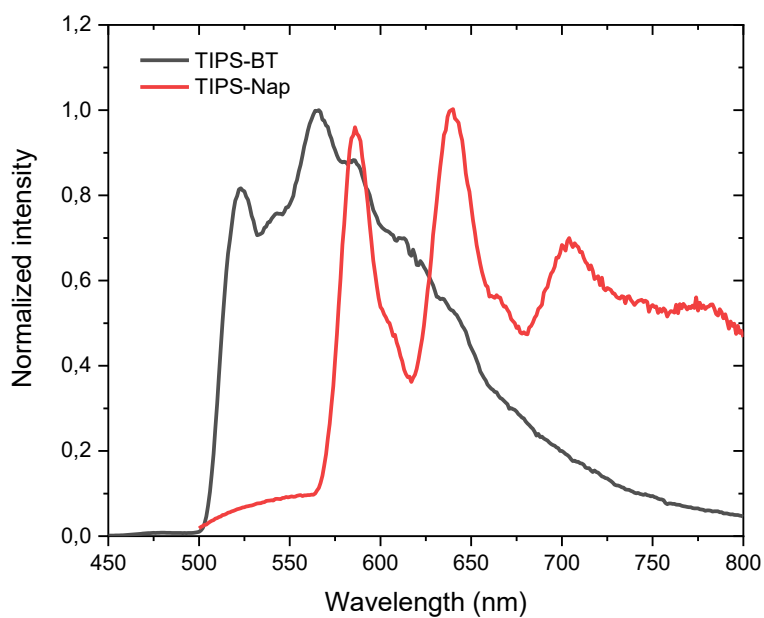


Figure S22: Phosphorescence spectra of TIPS-Nap and TIPS-BT in 2-methyl tetrahydrofuran at 77K in quartz tube. Sample was excited at 330 nm with 395 nm long pass filter placed across emission path. Data was collected after 0.05 ms of excitation pulse. Time between the excitation pulse of 61 ms.

NMR data

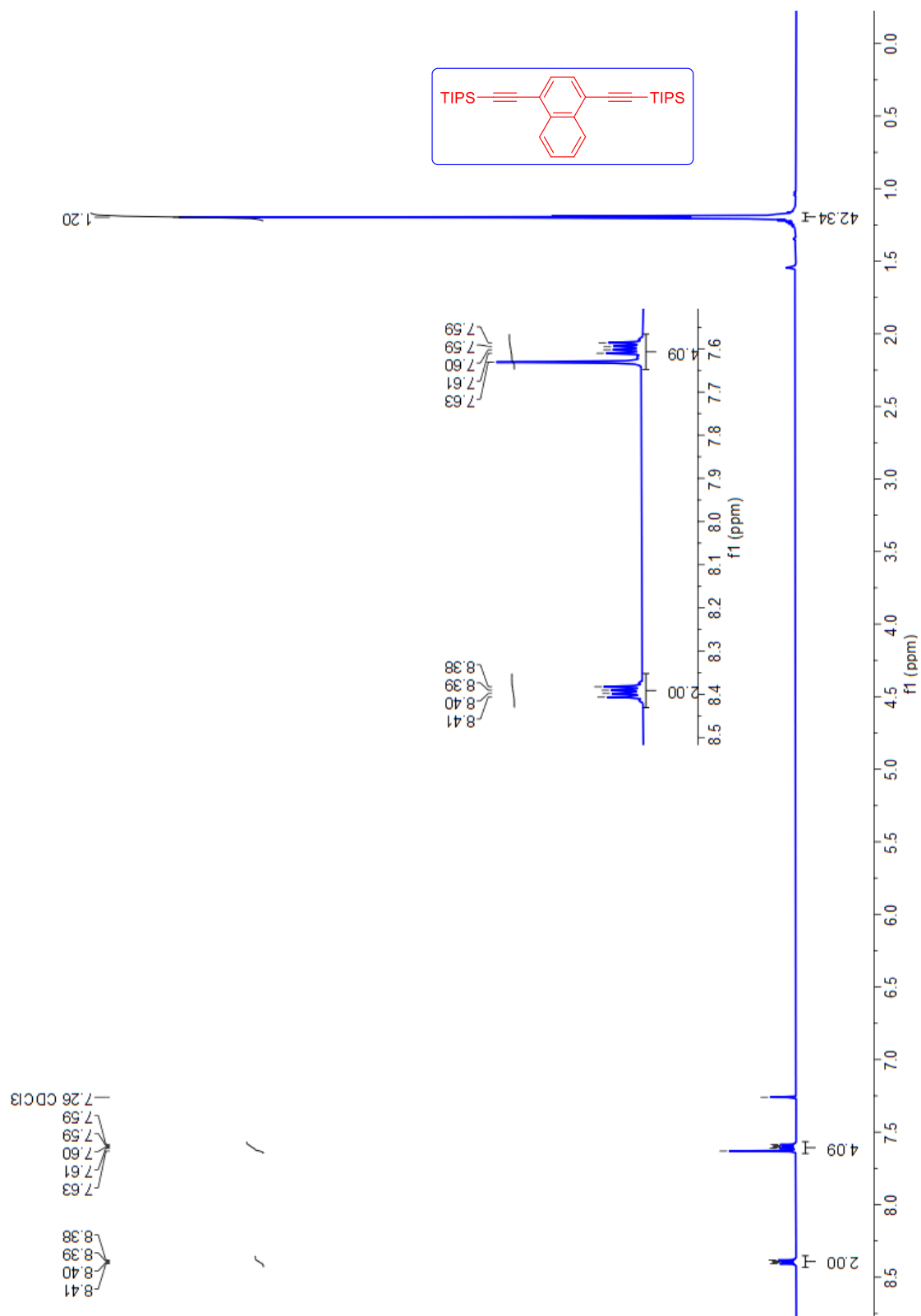


Figure S23: ¹H-NMR spectra of TIPS-Nap.

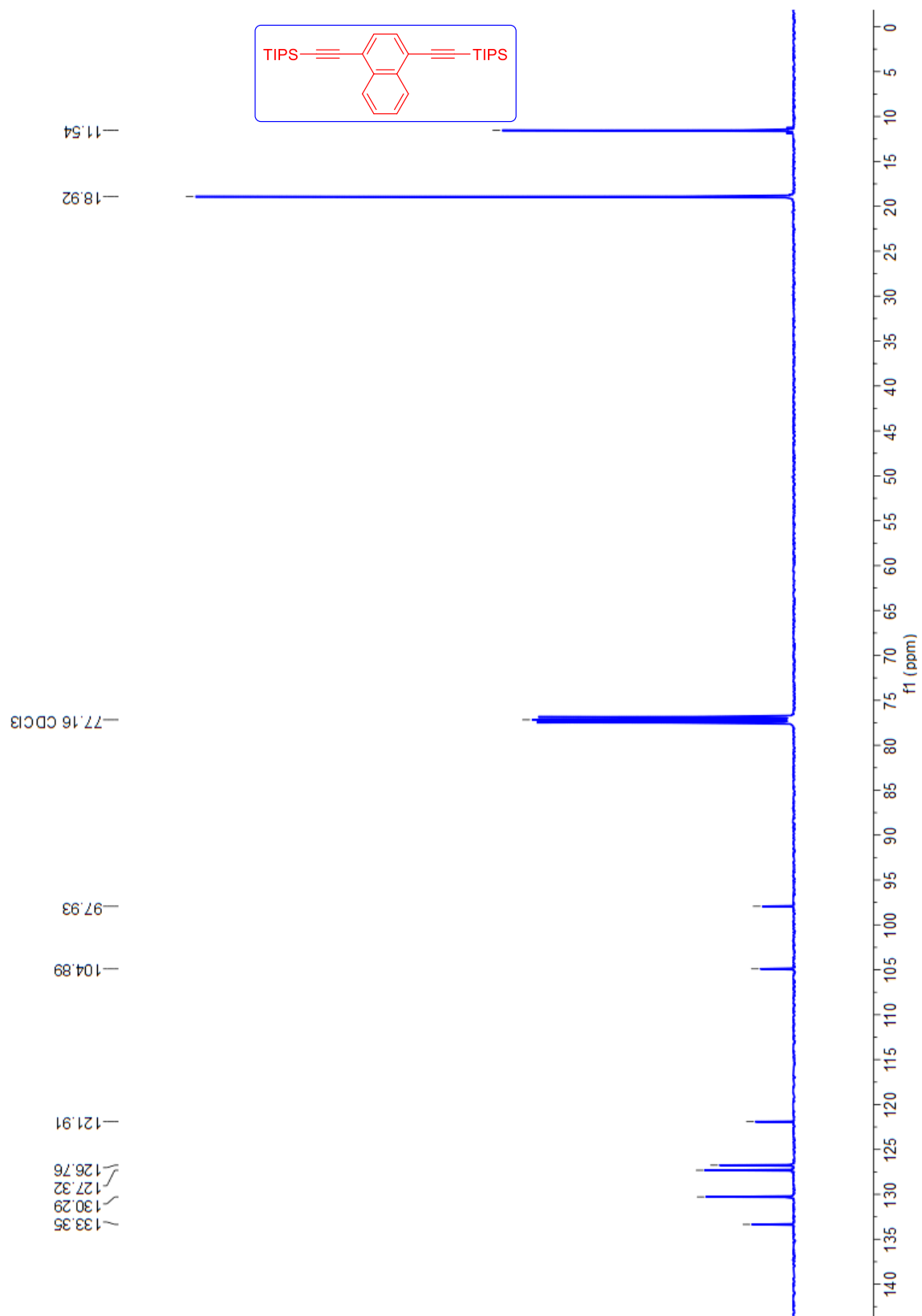


Figure S24: ¹³C-NMR spectra of TIPS-Nap.

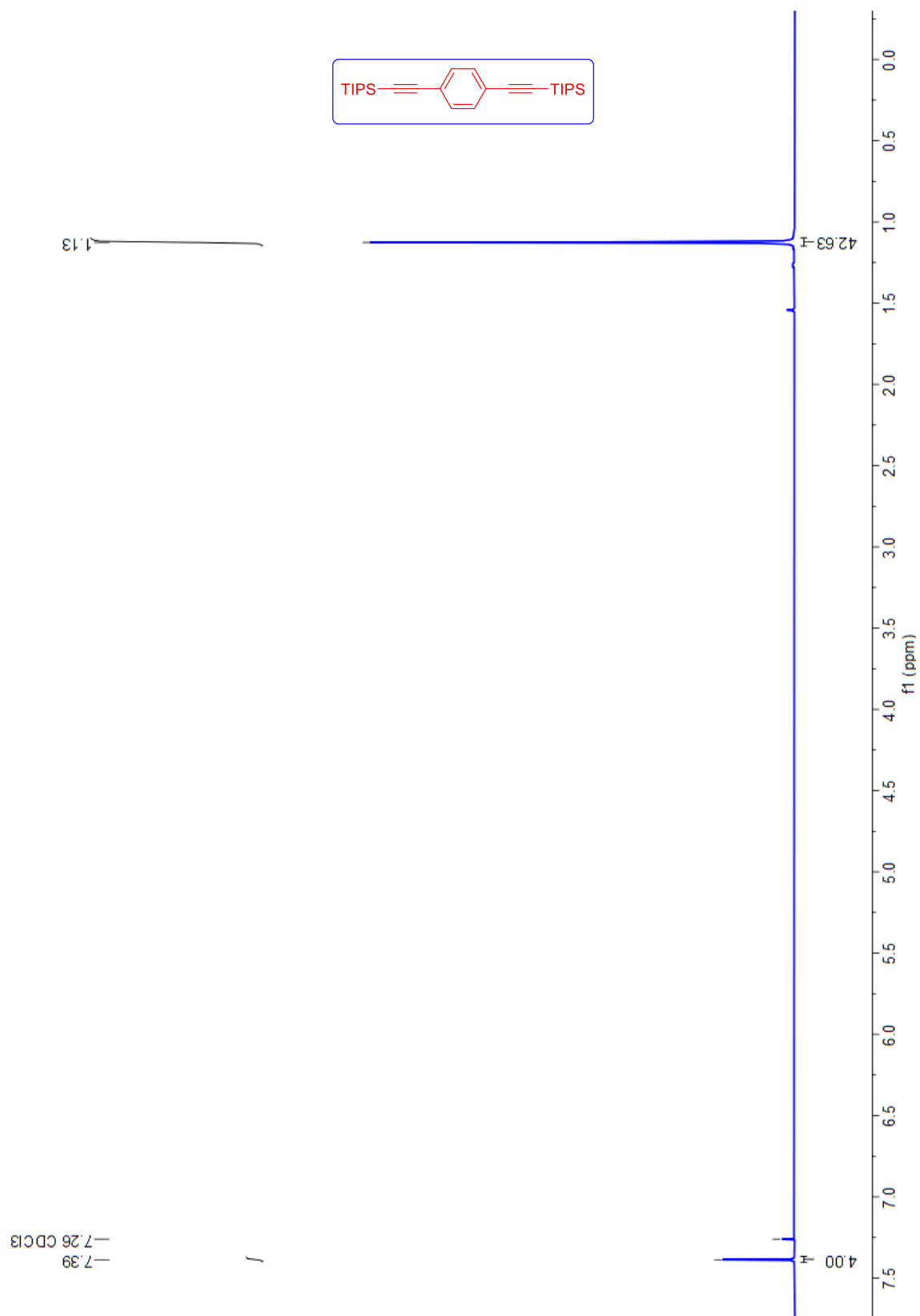


Figure S25: ¹H-NMR spectra of TIPS-Ph.

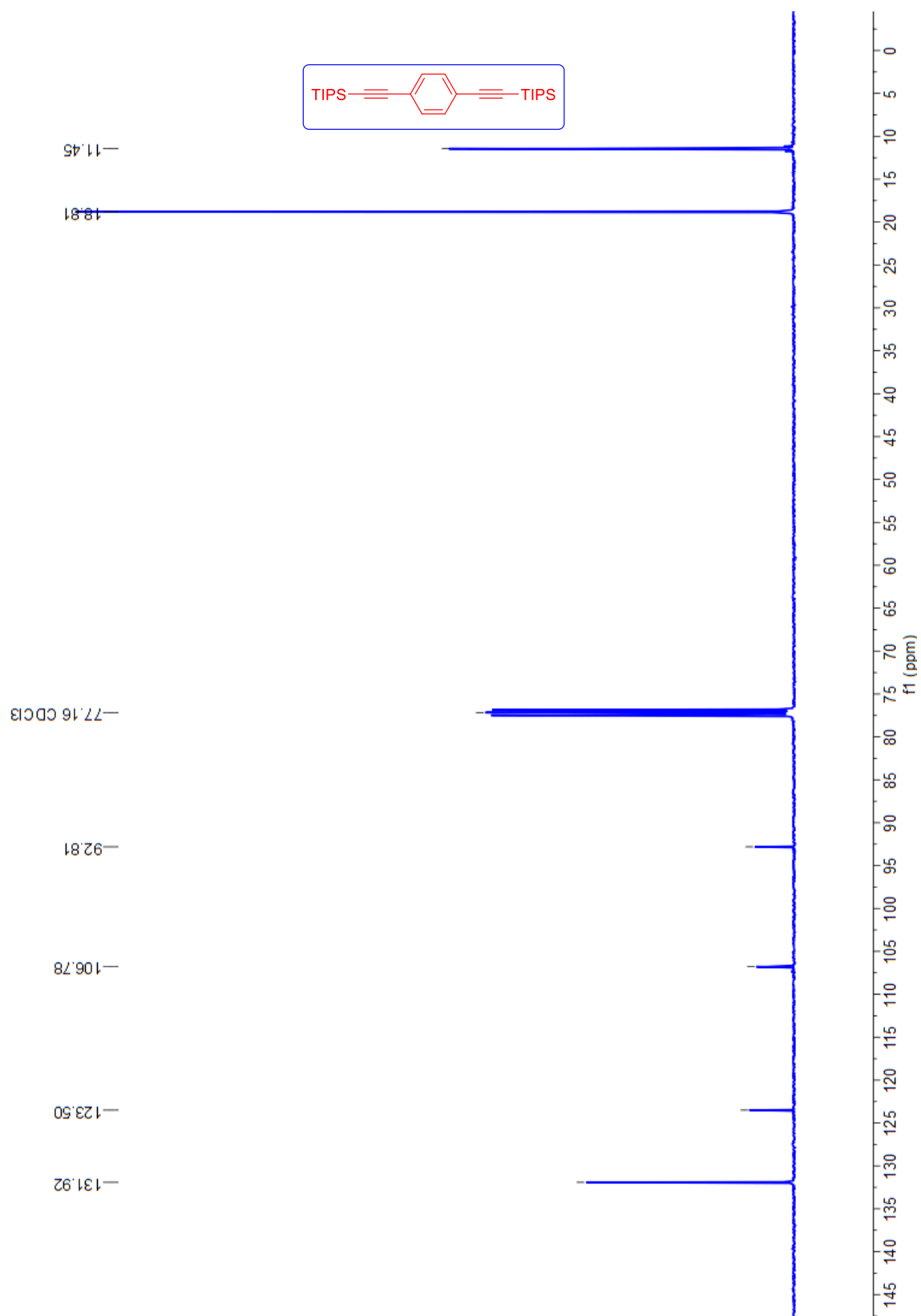


Figure S26: ^{13}C -NMR spectra of TIPS-Ph.

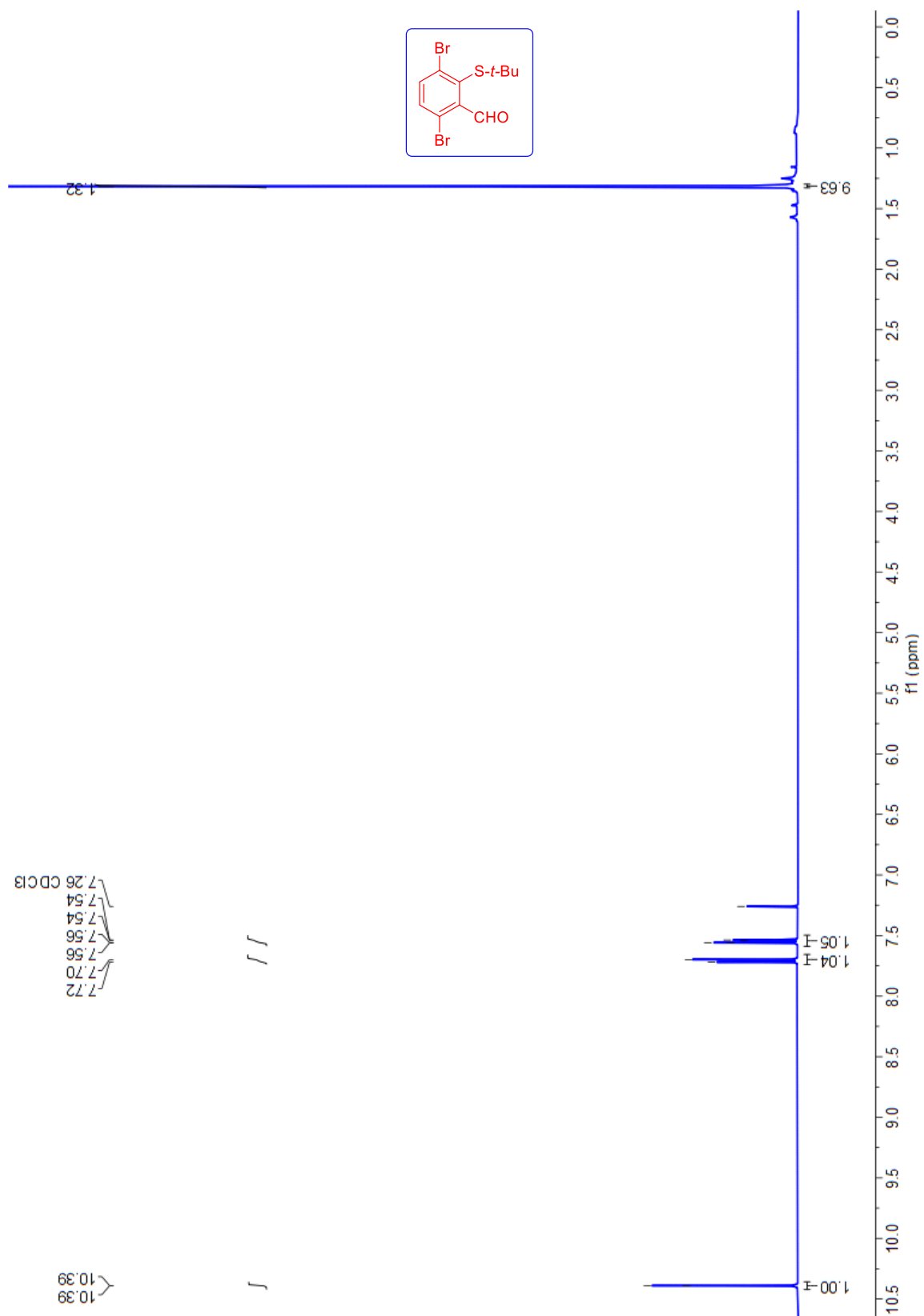


Figure S27: $^1\text{H-NMR}$ spectra of compound **3**.

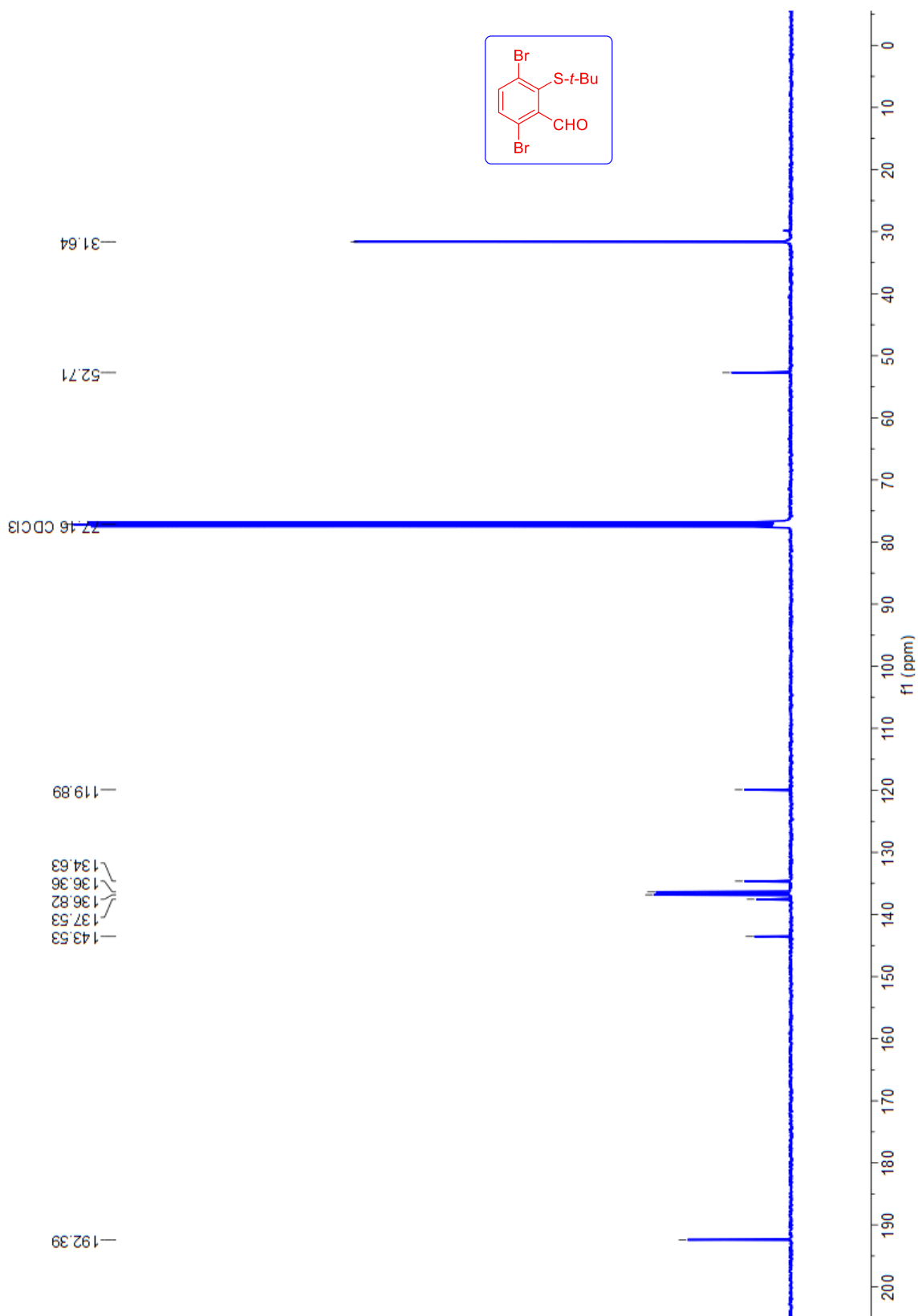


Figure S28: ¹³C-NMR spectra of compound 3.

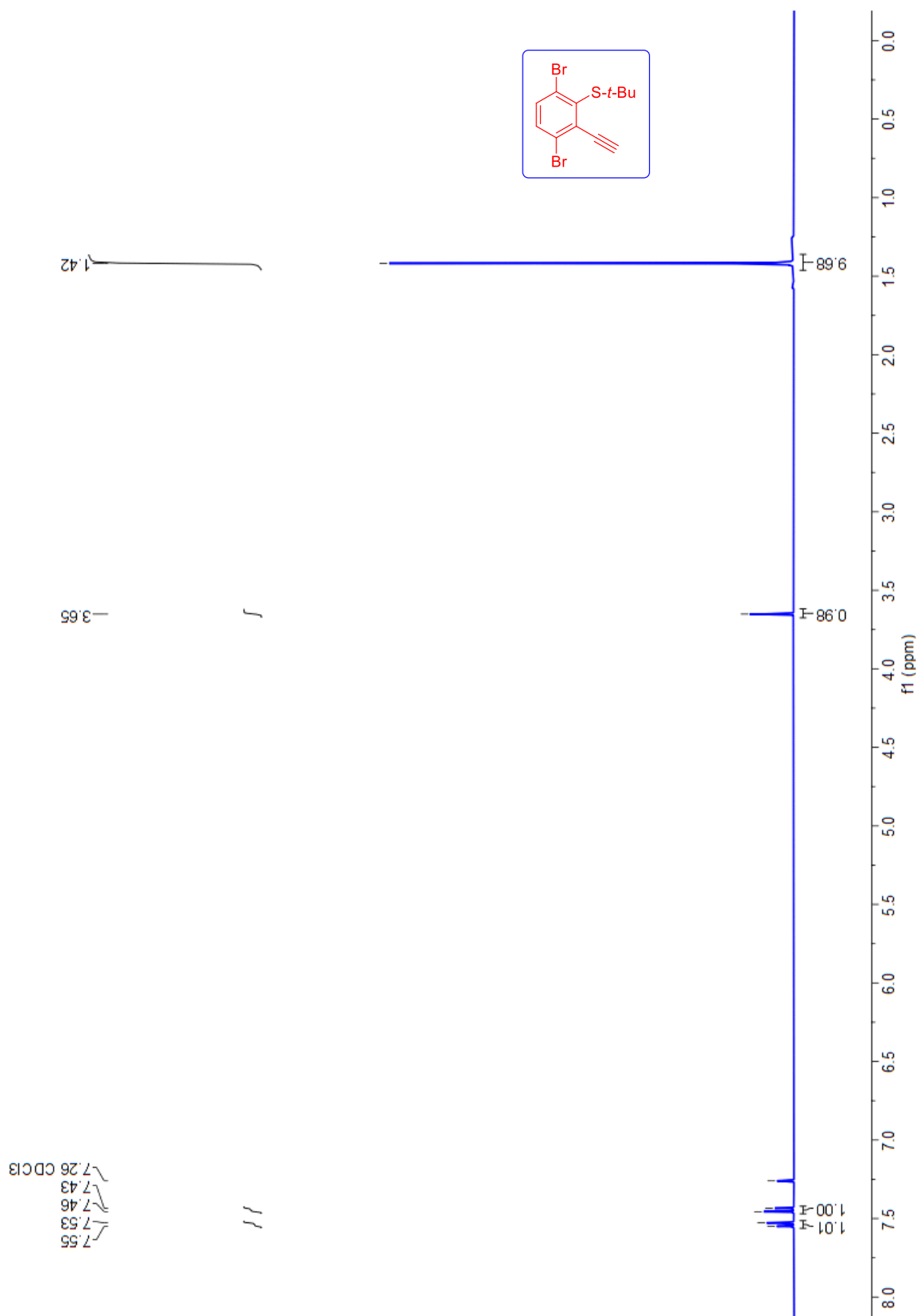


Figure S29: ¹H-NMR spectra of compound 4.

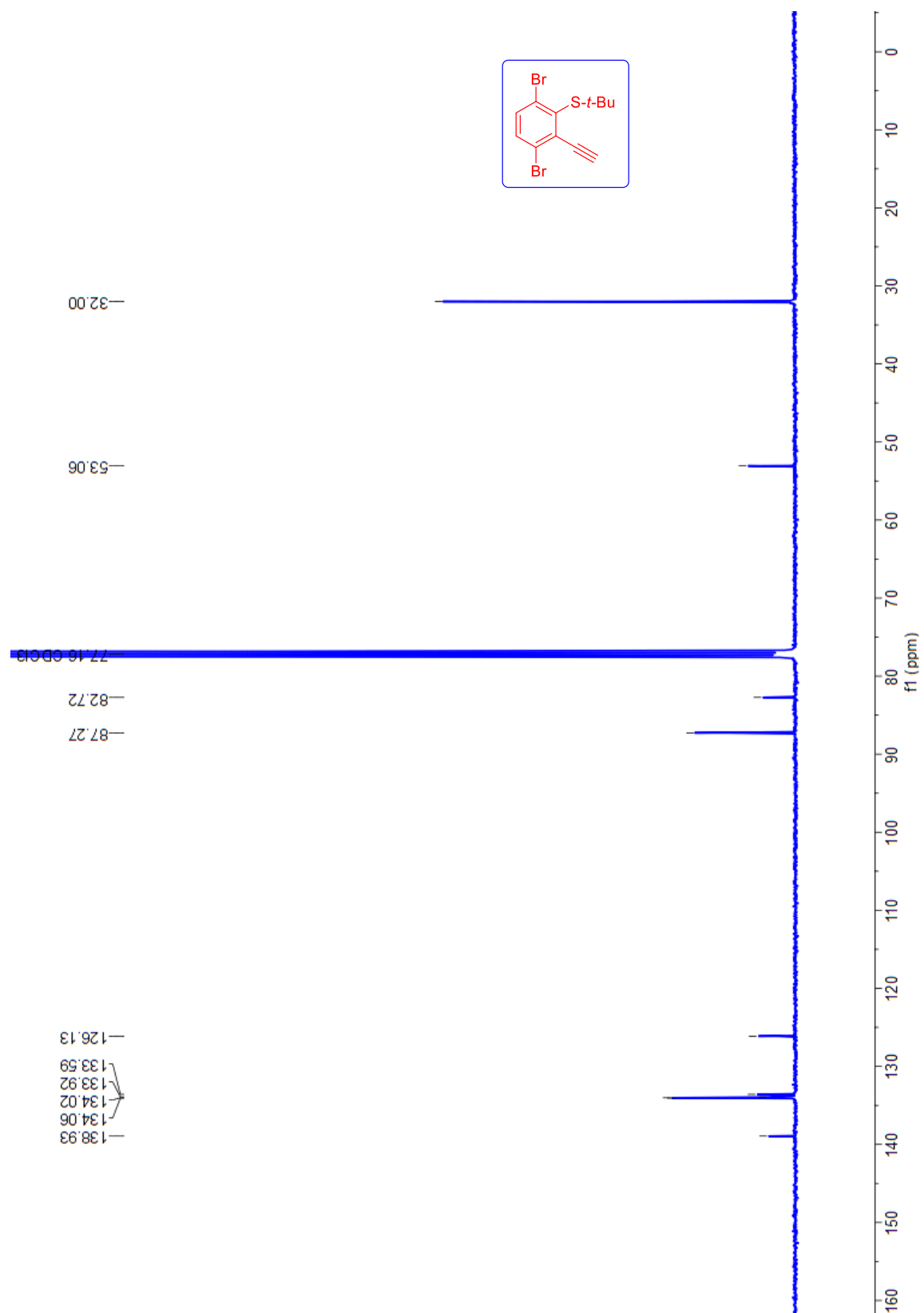


Figure S30: ¹³C-NMR spectra of compound 4.

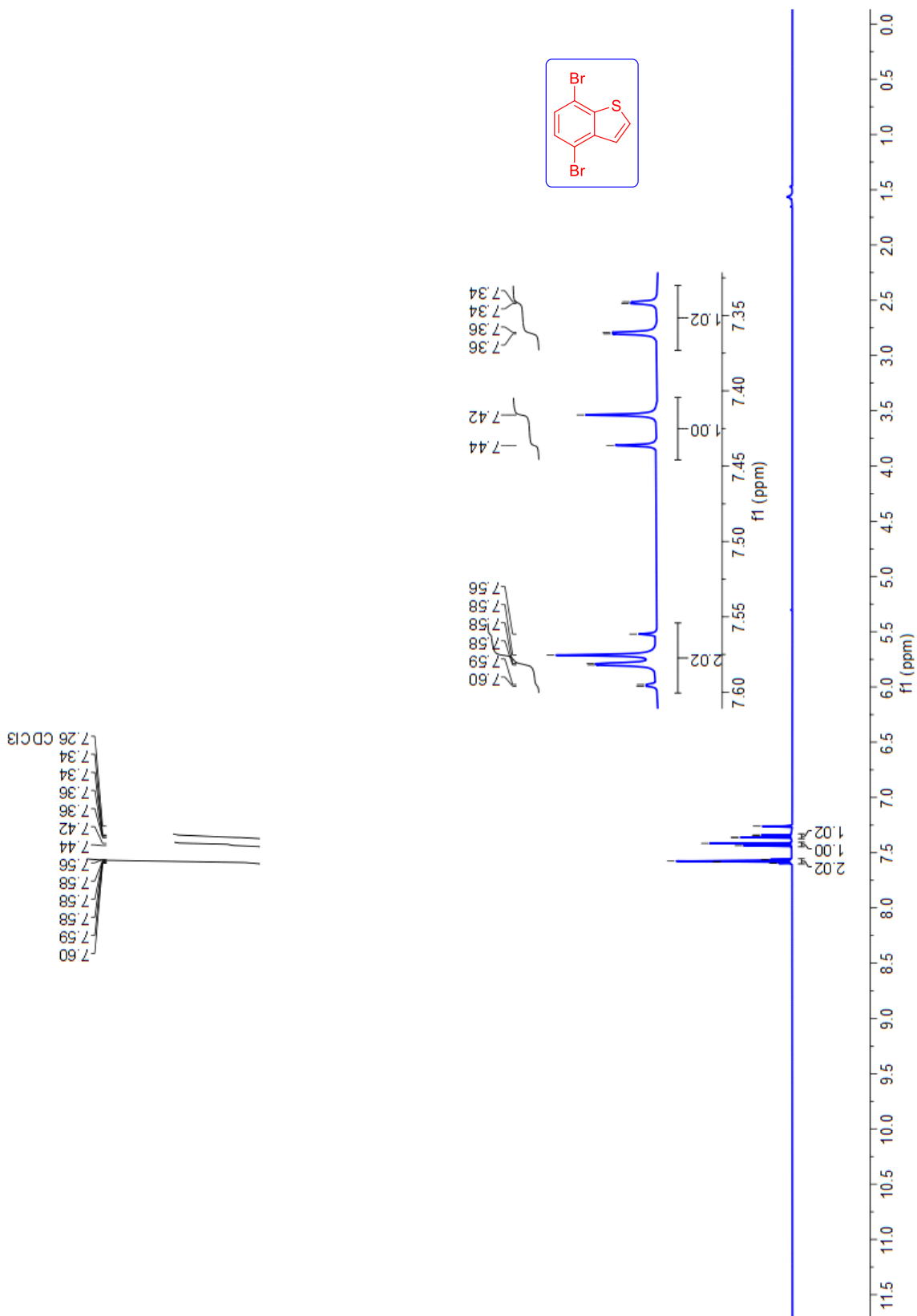


Figure S31: ¹H-NMR spectra of compound 5.

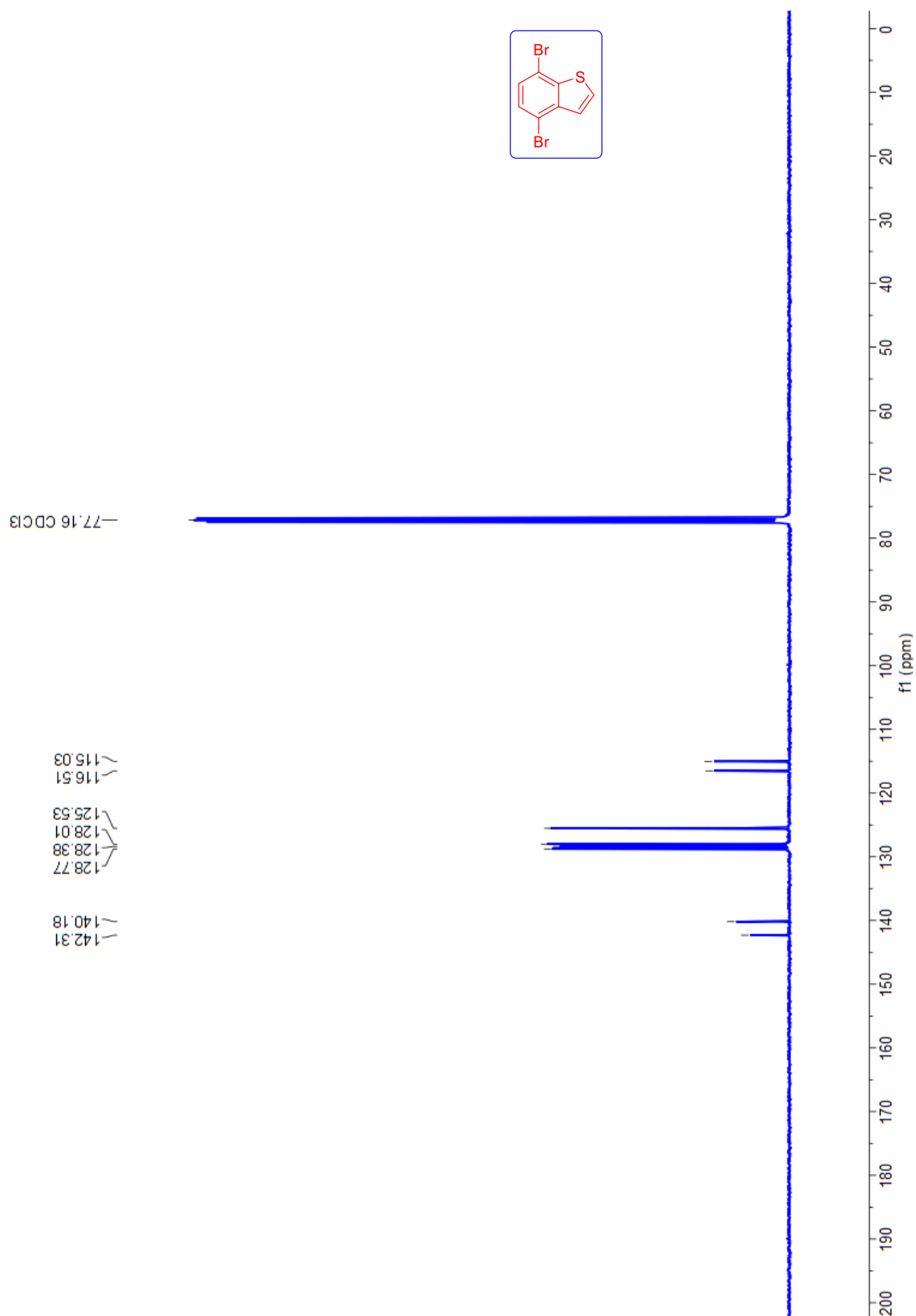


Figure S32: ^{13}C -NMR spectra of compound 5.

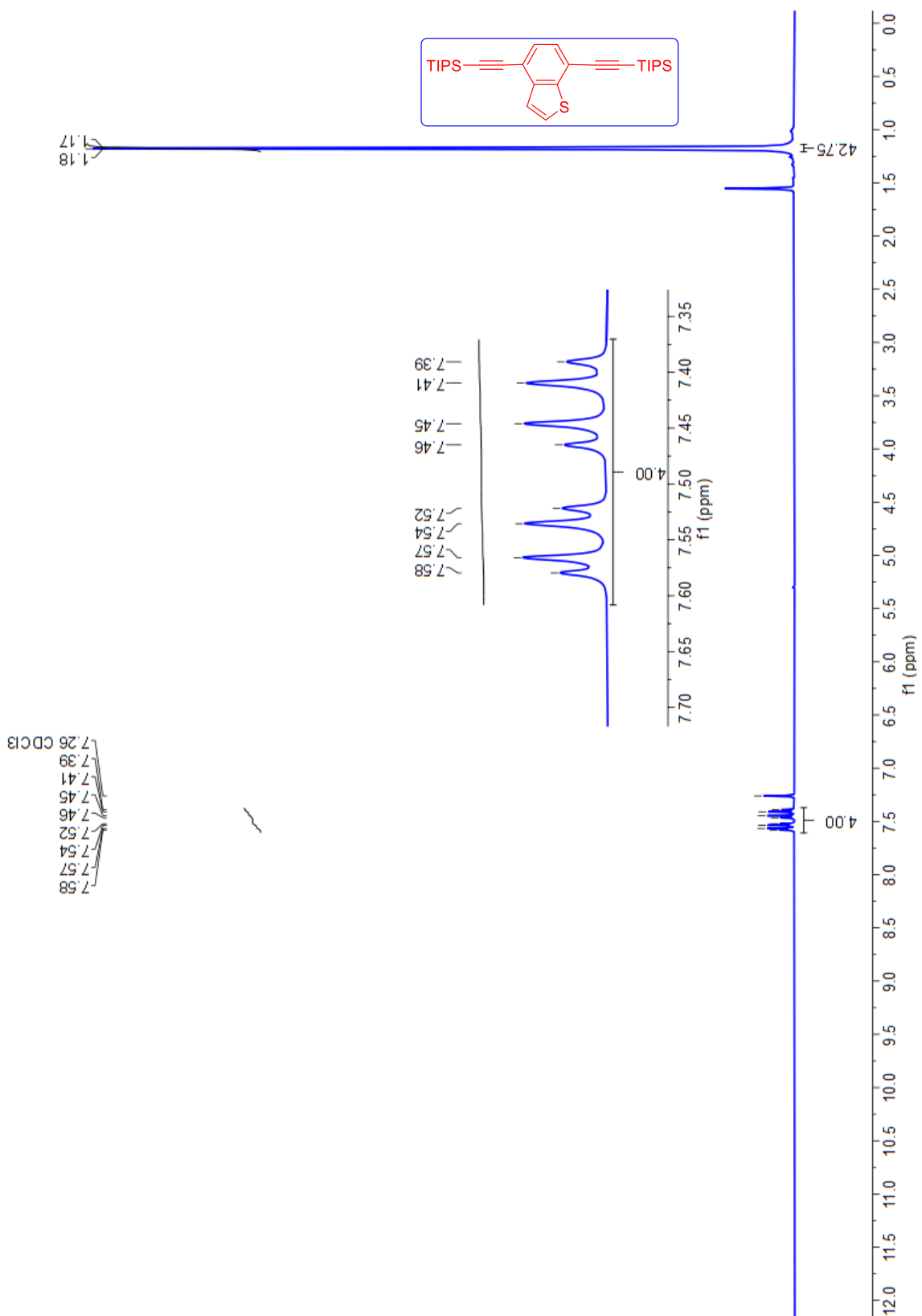


Figure S33: ¹H-NMR spectra of TIPS-BT.

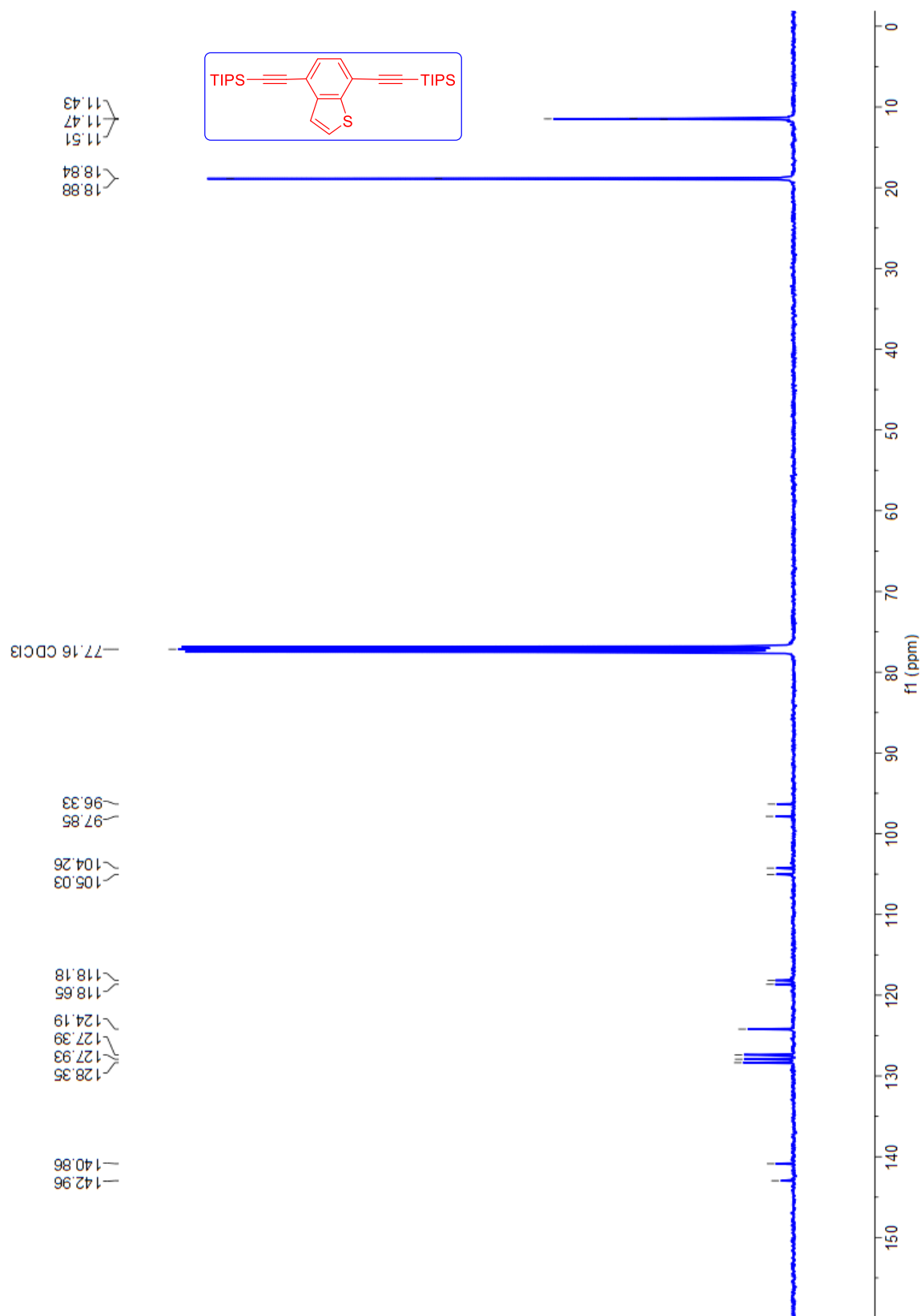


Figure S34: ¹³C-NMR spectra of TIPS-BT

Kinetic Modelling

Kinetic modelling was done using MATLAB. The code is available to download at the repository: [link-to-be-added-in proof](#)

The differential equations describing the trimolecular system used for the modelling are described below:

$$\frac{d[{}^3Sen^*]}{dt} = k_{Ex}[Sen] - k_S[{}^3Sen^*] - k_{TET}[{}^3Sen^*][M] - k_{TET}[{}^3Sen^*][A] \quad (1)$$

$$\frac{d[{}^3M^*]}{dt} = k_{TET}[{}^3Sen^*][M] - 2k_{TTA}^{homo}[{}^3M^*]^2 - k_T^M[{}^3M^*] - k_{TET}^{M \rightarrow A}[{}^3M^*][A] - k_{TTA}^{hetero}[{}^3M^*][{}^3A^*] + k_{bTET}^{A \rightarrow M}[{}^3A^*][M] \quad (2)$$

$$\frac{d[{}^1M^*]}{dt} = k_{TTA}^{homo}[{}^3M^*]^2 - k_{FL}^M[{}^1M^*] \quad (3)$$

$$\frac{d[{}^3A]}{dt} = k_{TET}[{}^3Sen^*][A] + k_{TET}^{M \rightarrow A}[{}^3M^*][A] - 2k_{TTA}^{homo}[{}^3A^*]^2 - k_T^A[{}^3A^*] - k_{TTA}^{hetero}[{}^3M^*][{}^3A^*] - k_{bTET}^{A \rightarrow M}[{}^3A^*][M] \quad (4)$$

$$\frac{d[{}^1A^*]}{dt} = k_{TTA}^{homo}[{}^3A^*]^2 + k_{TTA}^{hetero}[{}^3M^*][{}^3A^*] - k_{FL}^A[{}^1A^*] \quad (5)$$

$$\frac{d[M]}{dt} = k_{FL}^M[{}^1M^*] - k_{TET}[{}^3Sen^*][M] + k_{TET}^{M \rightarrow A}[{}^3M^*][A] + k_{TTA}^{homo}[{}^3M^*]^2 + k_T^M[{}^3M^*] - k_{bTET}^{A \rightarrow M}[{}^3A^*][M] + k_{TTA}^{hetero}[{}^3M^*][{}^3A^*] \quad (6)$$

$$\frac{d[A]}{dt} = k_{FL}^A[{}^1A^*] - k_{TET}[{}^3Sen^*][A] - k_{TET}^{M \rightarrow A}[{}^3M^*][A] + k_{TTA}^{homo}[{}^3A^*]^2 + k_T^A[{}^3A^*] + k_{bTET}^{A \rightarrow M}[{}^3A^*][M] \quad (7)$$

$$\frac{d[Sen]}{dt} = -k_{Ex}[Sen] + k_S[{}^3Sen^*] + k_{TET}[{}^3Sen^*][M] + k_{TET}[{}^3Sen^*][A] \quad (8)$$

Where Sen refers to sensitizer, M to mediator, A to annihilator and [...] denotes concentration. k_{Ex} is the rate constant for excitation (s^{-1}) obtained from the excitation photon flux ($\text{photon s}^{-1} \text{cm}^{-2}$) and absorption cross-section (α , cm^2), $k_{Ex} = \alpha \times \text{flux}$. k_S is the rate constant for sensitizer triplet decay (s^{-1}), k_{TET} and $k_{TET}^{M \rightarrow A}$ are the bimolecular rate constants ($s^{-1} \text{M}^{-1}$) for triplet energy transfer

from sensitizer and from mediator to annihilator, respectively. $k_{bTET}^{A \rightarrow M}$ is the bimolecular rate constant for back triplet energy transfer from annihilator to mediator estimated from the energy difference ($\Delta E = 0.26$ eV) between the mediator and annihilator triplet energies ($k_{bTET}^{A \rightarrow M} = k_{TET}^{M \rightarrow A} e^{\frac{-\Delta E}{k_b T}}$). k_{TTA}^{homo} and k_{TTA}^{hetero} are the bimolecular rate constants for homo and hetero TTA, respectively. k_{FL}^i is the rate constant of fluorescence (s^{-1}), and k_T^i the rate constant of triplet decay (s^{-1}), of compound i .

We use the built in MATLAB function `ode23s` to solve the set of differential equations with `kEx = 0` and an initial triplet sensitizer concentration estimated from the flash photolysis ground state bleach, to extract the population dynamics over time. The time range is divided into smaller ranges to ensure smooth solutions using `ode23s`. The same set of equations can be solved for the bimolecular systems by setting either the mediator or annihilator ground state concentration to 0 M. A least-square fitting routine using the MATLAB function `fminsearch` is employed to fit the bimolecular model to the corresponding flash photolysis traces of the annihilator and mediator triplet signals, respectively. The rate constant for homo TTA (k_{TTA}^{homo}) is used as fitting parameter and the triplet lifetime is calculated continuously from the experimentally determined threshold intensity and k_{TTA}^{homo} as described in the main text Equation 2. k_{TET} , k_S , and k_{FL}^i are determined from complimentary experiments. No other rate constants are required for the bimolecular fits. For the trimolecular models the same rate constants are used as obtained from the bimolecular fits, and values for $k_{TET}^{M \rightarrow A}$ and k_{TTA}^{hetero} are roughly estimated manually to ensure the model best reproduces the experimental flash photolysis data.

For steady-state solutions we use the same set of equations and set them equal to 0, with the same rate constants as discussed above we use the built in MATLAB function `fsolve` to determine the steady-state concentrations of each species. The steady-state upconversion quantum yields of the annihilator (Φ_{UC}^A) and mediator (Φ_{UC}^M) are then calculated from the steady-state concentrations as per the equations below:

$$\Phi_{UC}^A = \frac{0.45 k_T [^1A^*]}{k_{Ex} [Sen]} \quad (9)$$

$$\Phi_{UC}^M = \frac{0.37 k_T [^1M^*]}{k_{Ex} [Sen]} \quad (10)$$

The prefactors 0.45 and 0.37 are the spin-factors determined for the bimolecular systems obtained by matching the modelled quantum yield to the experimentally obtained quantum yield.

Figures from kinetic modelling

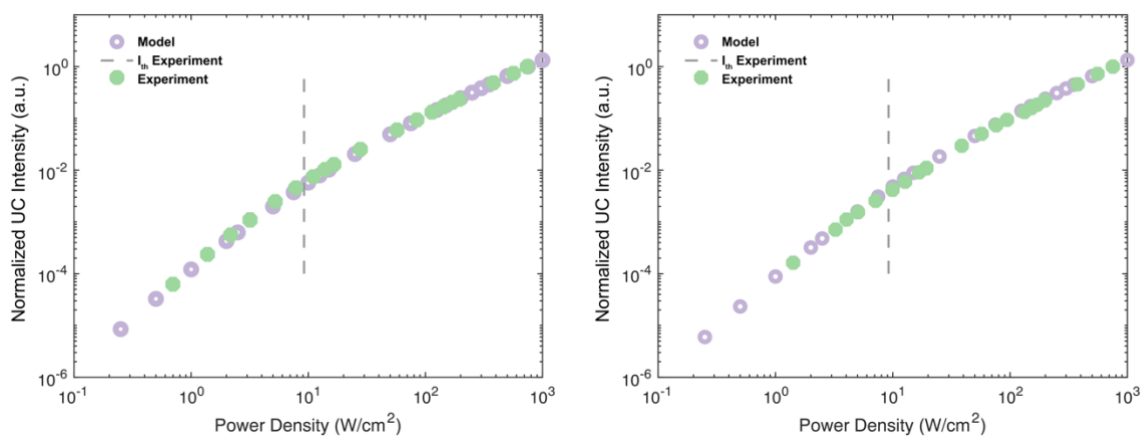


Figure S35: Experimental and modelled UC intensity dependence with 25 μM 4CzBN and 1mM TIPS-Nap (left) or 1mMTIPS-BT (right).

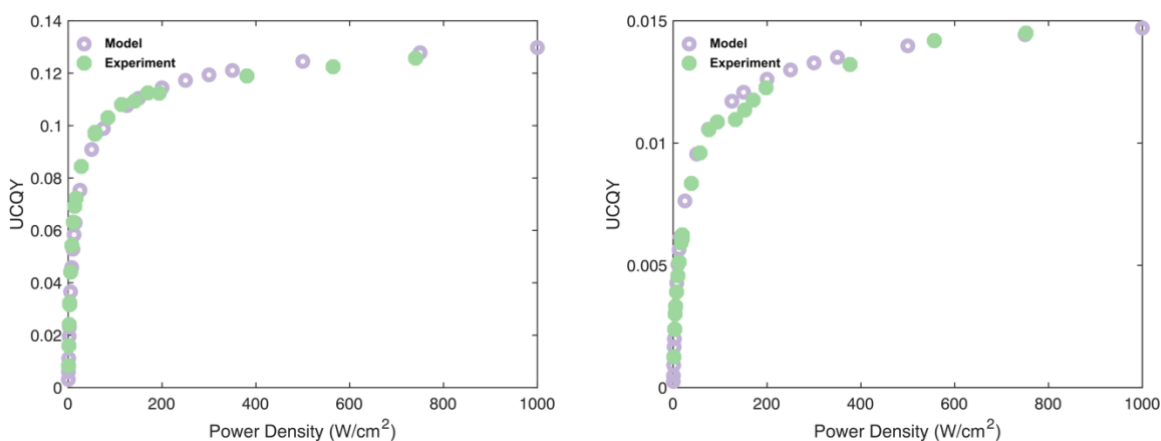


Figure S36: Experimental and modelled TTA-UC QYs with 25 μM 4CzBN and 1mM TIPS-Nap (left) or 1mMTIPS-BT (right) at different excitation power densities.

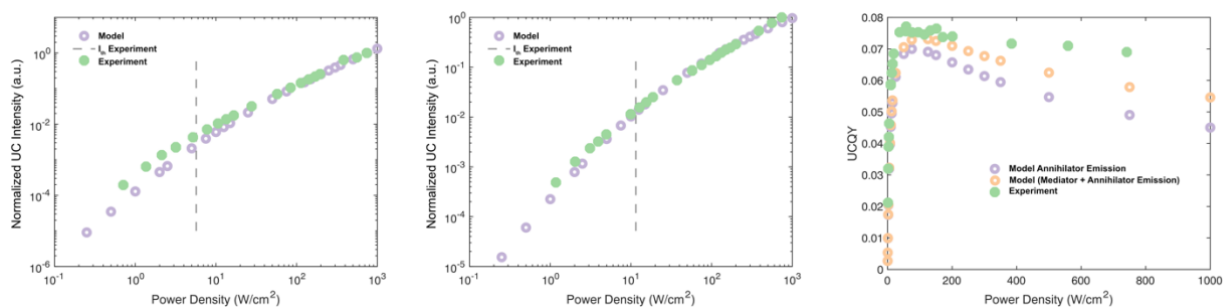


Figure S37: Experimental and modelled TTA-UC intensity dependence (left and center) and QYs (right) for 25 μM 4CzBN, 1mM mediator TIPS-BT and 0.1 mM (left) or 0.01 mM (center and right) TIPS-Nap at different excitation power densities

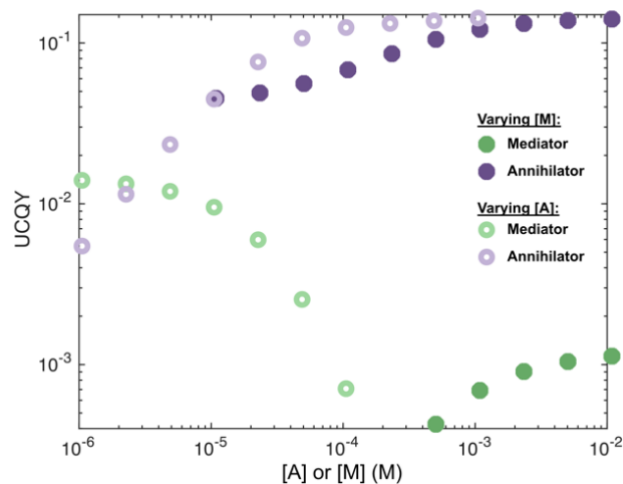


Figure S38: Modelled effect on the TTA-UC QY for annihilator and mediator emission, respectively, as a function of annihilator (open) and mediator (filled) concentration. For variations in annihilator concentration the mediator concentration is kept at 1 mM and for variations in mediator concentration the annihilator is kept at 0.1 mM. All rate constants are used as determined in the main manuscript and in the models above.

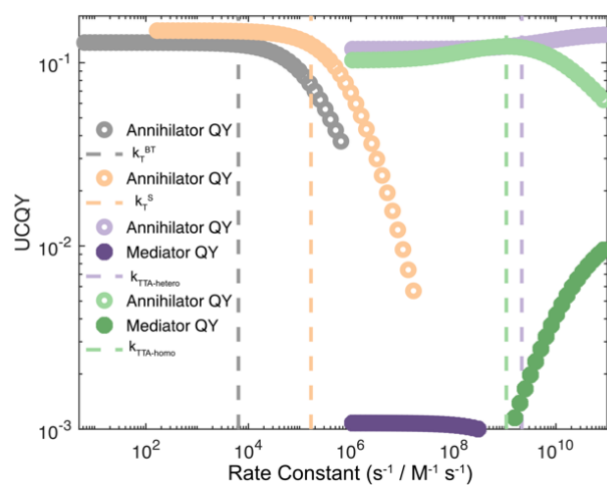


Figure S39: Modelled effect of the TTA-UC quantum yield for annihilator (open) and mediator (closed) emission, respectively, as a function of different rate constants. Dashed lines show the experimentally determined value for the rate constant in question for the current 25 μM 4CzBn/1mM TIPS-BT/0.1mM TIPS-Nap system.

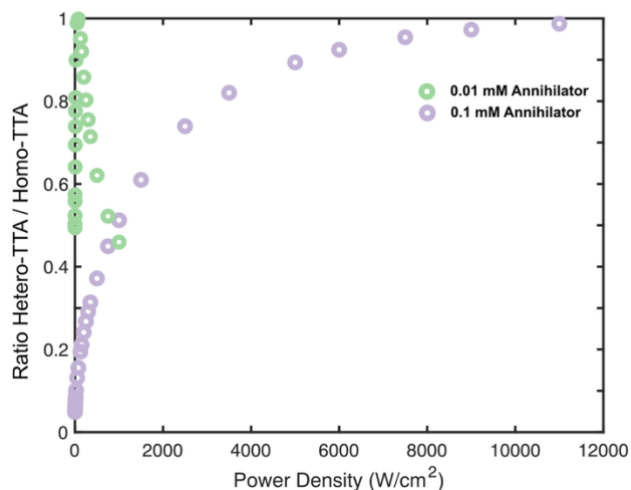


Figure S40: The ratio of hetero-TTA and the sum of annihilator and mediator homo-TTA as a function of excitation power density for low (0.01 mM, green) and high (0.1 mM, purple) concentrations of annihilator.

References

- 1 G. R. Fulmer, A. J. M. Miller, N. H. Sherden, H. E. Gottlieb, A. Nudelman, B. M. Stoltz, J. E. Bercaw and K. I. Goldberg, *Organometallics*, 2010, **29**, 2176–2179.
- 2 R. J. Armstrong, W. Niwetmarin and V. K. Aggarwal, *Org. Lett.*, 2017, **19**, 2762–2765.
- 3 N. Harada, Y. Sasaki, M. Hosoyamada, N. Kimizuka and N. Yanai, *Angewandte Chemie International Edition*, 2021, **60**, 142–147.
- 4 T. Yamamoto, H. Katsuta, K. Toyota, T. Iwamoto and N. Morita, *Bulletin of the Chemical Society of Japan*, 2012, **85**, 613–623.
- 5 C. Würth, M. Grabolle, J. Pauli, M. Spieles and U. Resch-Genger, *Nature Protocols*, 2013, **8**, 1535–1550.
- 6 M. Levitus, *Methods and Applications in Fluorescence*, 2020, **8**, 033001.
- 7 A. Olesund, J. Johnsson, F. Edhborg, S. Ghasemi, K. Moth-Poulsen and B. Albinsson, *J. Am. Chem. Soc.*, 2022, **144**, 3706–3716.
- 8 Y. Zhou, F. N. Castellano, T. W. Schmidt and K. Hanson, *ACS Energy Lett.*, 2020, **5**, 2322–2326.
- 9 A. Olesund, V. Gray, J. Mårtensson and B. Albinsson, *J. Am. Chem. Soc.*, 2021, **143**, 5745–5754.
- 10 J. I. Day, K. N. Allen-Moyer and K. P. Cole, *J. Org. Chem.*, 2023, **88**, 4209–4223.
- 11 Z. Alassad, A. AboRaed, M. S. Mizrachi, M. H. Pérez-Temprano and A. Milo, *J. Am. Chem. Soc.*, 2022, **144**, 20672–20679.
- 12 S. Wu, L. A. Galán, M. Roux, F. Riobé, B. Le Guennic, Y. Guyot, T. Le Bahers, L. Micouin, O. Maury and E. Benedetti, *Inorg. Chem.*, 2021, **60**, 16194–16203.
- 13 A. Olesund, J. Johnsson, F. Edhborg, S. Ghasemi, K. Moth-Poulsen and B. Albinsson, *J. Am. Chem. Soc.*, 2022, **144**, 3706–3716.